Spatiotemporal dynamics of human attention revealed by intracerebral recording

One-sentence summary (125 characters max)

The neural basis of human exogenous attention lies in the nexus between perception and action

Tal Seidel Malkinson[1], Dimitri J. Bayle[2], Alexia Bourgeois[3], Katia Lehongre[4], Sara Fernandez[4], Vincent Navarro[1,5,6], Claude Adam[1,5,6], Daniel Margulies[7], Jacobo D. Sitt[1], and Paolo Bartolomeo[1] *

[1] Sorbonne Université, Inserm UMRS 1127, CNRS UMR 7225, Paris Brain Institute, ICM, Hôpital de la Pitié-Salpêtrière, F-75013 Paris, France
[2] Centre de Recherche sur le Sport et le Mouvement (CeRSM, EA 2931), Université Paris Ouest-La Défense., F-92000 Nanterre, France
[3] Laboratory of Cognitive Neurorehabilitation, Faculty of Medicine, University of Geneva, 1206 Geneva, Switzerland
[4] CENIR - Centre de Neuro-Imagerie de Recherche, Paris Brain Institute, ICM, Hôpital de la Pitié-Salpêtrière, F-75013 Paris, France
[5] Service de neurologie 1, Hôpital de la Pitié-Salpêtrière, F-75013 Paris, France
[6] Service de Neurophysiologie Clinique, Hôpital de la Pitié-Salpêtrière, F-75013 Paris, France
[7] Laboratoire INCC, équipe Perception, Action, Cognition, Université de Paris, F-75005 Paris, France

ABSTRACT. Attention allows us to rapidly respond to unexpected events, a fundamental capacity for survival. We recorded brain activity from 28 individuals with a total of 1,403 intracortical contacts, while they produced faster manual responses to visual targets preceded by non-predictive attentional cues, which engage exogenous spatial attention. Using a novel spatiotemporal clustering approach, we identified three distinct brain networks: an early visual cluster; an intermediate, predominantly right-hemisphere caudal temporoparietal-prefrontal cluster, sensitive to attentional effects; and a late, predominantly left-hemisphere rostral temporoparietal-prefrontal cluster, sensitive to response-requiring targets. Activity in temporoparietal-prefrontal clusters suggested neural integration of temporally close cues and targets, and was closely related to behavioral responses. These results reveal how cortical networks govern the psychological construct of exogenous attention.

Imagine yourself on the point of crossing a busy street. To safely reach the other side, you need to successfully integrate potentially competing sources of information. You have to pay attention to the traffic light for the 'go' signal to appear, while also being able to respond to unforeseen and potentially dangerous events, such as an accelerating car suddenly approaching. Attentional processes resolve these conflicting goals. Attention can be guided by a person's goals (endogenous orienting: monitoring the traffic light), but also captured by a salient external stimulus (exogenous orienting: looking at the approaching car). However, the timing of exogenous attention critically depends on slight differences in the delay between events. When successive visual events, such as an attentional cue and a target, appear at the same spatial

---

* *Contributions:*
TSM: conceptualization, investigation, software, formal analysis, writing - original draft preparation, visualization, project administration, funding acquisition. DJB: conceptualization, investigation, software. AB: software. KL: resources, investigation. SF: resources, software. VN: resources. CA: resources. DM: resources, writing - reviewing and editing, software. JDS: conceptualization, software, writing - reviewing and editing. PB: Supervision, writing - reviewing and editing, funding acquisition.

location with short delays, the cue tends to speed target detection, resulting in shorter response times (*RT facilitation*). Slightly longer delays, however, slow down target detection, a phenomenon termed *inhibition of return* (IOR) (*1*, *2*). Despite decades of research, the nature and underlying neural mechanisms that mediate these behavioral effects remain unclear (*3*, *4*). Evidence from human (*5*) and non-human studies (*6*) suggest an important role for the midbrain superior colliculus (SC) in IOR. However, IOR does not originate in the SC (*6*), is likely to reflect cortical influence, for example of the posterior parietal cortex (PPC) and the frontal eye field (FEF) (*7*–*11*). Moreover, in human patients with spatial neglect resulting from right hemisphere damage (especially to the supramarginal gyrus or to its connections with the ipsilateral prefrontal cortex (*12*)), manual IOR is decreased in the right, non-neglected hemi-field (*13*, *14*), and may enable an abnormal faster detection of right-sided repeated targets than non-repeated ones, i.e., *facilitation of return* (*12*). Yet, the emerging understanding of these attentional processes remain fragmented, leaving the implicated cortical networks and underlying mechanism unclear.

Here we used intracerebral electroencephalography (iEEG), a technique with unmatched spatiotemporal resolution in humans (*15*), to determine the brain dynamics of the mechanisms implicated in the exogenous orienting of spatial attention. Twenty-eight participants undergoing presurgical evaluation of their epilepsy with iEEG (age 31.7 ± 8.1 years, 15 women, Table 1) performed the Posner peripheral cueing task (*2*) (Fig. 1A). Participants were asked to detect the appearance of a target within a right-sided or a left-sided placeholder as quickly as possible. A non-predictive peripheral cue preceded the target with two possible stimulus onset asynchronies (SOA): 150ms (short-SOA), or 600ms (long-SOA), and appeared either on the same side of the target (Congruent trials) or opposite side (Incongruent trials) with equal probability. Patients' performance was neurotypical, with a 30-ms IOR effect (Fig. 1B; 2-way-ANOVA: SOA × Congruence interaction, $F_{(1,27)}=39.50$, $p<0.001$, $\eta^2 = 0.164$; post-hoc test: long-SOA congruent vs. Incongruent $p<0.001$). Congruent and incongruent RTs differed between SOAs (post-hoc tests: $p=0.047$ and $p=0.008$, respectively), but facilitation at short-SOA failed to reach significance (p=0.37; see Fig. S1 for individual RTs), as is often the case with this delicate effect (*16*).

High-frequency broadband power (55-145Hz; HFBB) was recorded from 1403 usable contacts with bipolar montage (Fig. 1C; See Table 2 for detailed localization). Target-locked mean normalized HFBB activity was extracted for each contact in the eight experimental conditions (2x2x2 design: SOA x Congruence x Ipsilateral/Contralateral target related to contact; Fig. 1C).

In order to reveal the main temporal patterns of activity that were sensitive to the experimental manipulations, we used a customized clustering approach, the trajectory K-means clustering (Fig. S2), which we applied to 664 responsive contacts (with at least 100ms-long significant effect in one condition or more, compared to baseline). We calculated the temporal trajectory in the 8-dimensional condition space (Congruent / Incongruent Trial X short-SOA / long-SOA X Ipsilateral / contralateral target) for each of the responsive contacts, which was then assigned to the cluster with the nearest trajectory-centroid, by iteratively minimizing within-cluster Manhattan distances.

Out of the optimal 6-cluster solution (Fig S2A-C), we identified three clusters of contacts whose activity patterns changed across the experimental conditions (Fig. 1D). The first cluster (Visual cluster; 68 contacts; Fig. 1D right) showed early responses only to contralateral cues and targets, and mainly consisted of contacts in the occipitotemporal cortex and in the prefrontal cortex, around the FEF (Fig. 1E top). A second cluster (Caudal temporoparietal junction (TPJ) - Prefrontal cluster; 97 contacts; Fig. 1D middle) showed later bilateral activity, with stronger responses to contralateral stimuli. Most contacts were in the caudal portion of the TPJ, around the angular gyrus, posterior temporal cortex and prefrontal cortex (Fig. 1E

middle). The cluster was lateralized to the right hemisphere (Fig. S2D-E). The third cluster (Rostral TPJ - Prefrontal cluster; 67 contacts; Fig. 1D left) was the latest to intervene, with stronger responses to bilateral targets than to cues. It was located mainly in the rostral TPJ region (around the supramarginal gyrus), posterior temporal cortex and prefrontal cortex (Fig. 1E bottom), and was lateralized to the left hemisphere (Fig. S2 D-E). Importantly, the response in the Caudal TPJ-Prefrontal and the Rostral TPJ-Prefrontal clusters was sensitive to the cue-target delay. For the short-SOA, cue and target responses were summed together, but for the long-SOA they were segregated. These clusters were further investigated. The activity of the remaining three clusters was similar across experimental conditions, with one cluster showing late inhibition, one showing late activation and one showing no response.

We Next examined IOR-related activity, by comparing between Congruent and Incongruent trials with long SOA (time-resolved 3-way ANOVA; Fig. 2). The Caudal TPJ-Prefrontal cluster showed a Congruence effect at the offset of the target-related activity (240-300ms post target; all $p<0.002$; see Fig. 2D for examples of single contacts). Moreover, in the contacts of this cluster in the right hemisphere, the response peaked 22ms earlier in the Incongruent than in the Congruent trials (140-220ms post target onset; Hemisphere x Congruence interaction: all $p<0.03$; post hoc tests: all $p<0.014$), mirroring behavioral IOR. The activity in the Visual cluster did not show any congruence effects (Fig. 2A); the Rostral TPJ-Prefrontal cluster showed only a late Congruence effect at 660-680ms post-target (all $p<0.003$). Therefore, IOR-related activity was mainly restricted to the Caudal TPJ-Prefrontal cluster.

How do these clusters of neural activity relate to behavior? In each cluster, we divided the trials (pooled across conditions) into 20 quantiles according to their RT (Fig. 3A), and tested the relation of RT-bins with the neural activity using a time-resolved 1-way repeated measures ANOVA (See Fig. 3B-C for results and examples of single contacts). In the Caudal TPJ-Prefrontal cluster, the offset of the target-related activity differed across RT bins (300-560ms post target; all $p<0.028$), with a faster decay at faster RT-bins, just before the motor response. In the Rostral TPJ-Prefrontal cluster, an RT-bin effect occurred around the peak of target-related activity and button-press time (280-300 and 400-0420ms post target; all $p<0.007$). In the Visual cluster, an RT-bin effect occurred at 500-540 and 560-680ms post target onset ($p<0.002$), suggesting an RT-related late modulation after response offset and button press time. RT-related target-locked activity in the Caudal TPJ-Prefrontal and Rostral TPJ-Prefrontal clusters was confirmed by cross-correlation analysis (Fig. S3), which revealed that only in these clusters did the temporal dynamics of neural activity shift according to RTs, and that this shift correlated with RTs.

We next adopted a complementary perspective, and examined the visual modulation of response-locked activity. We applied the trajectory k-means clustering analysis to response-locked activity (Fig. S4 A-C). A contingency analysis revealed four clusters of contacts, corresponding to the previously identified target-locked clusters ($X^2_{(30)}=1442$; $p<0.001$; Contingency coefficient, 0.83; Fig. 3 and S4D). Specifically, analysis of response-locked activity teased apart early and late activity clusters: an Early visual cluster (46 contacts; 60.3% of Visual target-locked cluster), an Early Caudal TPJ-Prefrontal cluster (85 contacts; 35.3% of Visual and 49.5% Caudal TPJ-Prefrontal target-locked clusters), a Late Caudal TPJ-Prefrontal cluster (79 contacts; 46.4% of Caudal TPJ-Prefrontal and 31.3% of Rostral TPJ-Prefrontal target-locked clusters), and a Late Rostral TPJ-Prefrontal (39 contacts; 50.7% of Rostral TPJ-Prefrontal target-locked clusters). Neural activity in the Early and Late Caudal TPJ-Prefrontal clusters was IOR-related (Fig. S5). We repeated the RT-binning analysis, dividing the trials (pooled across conditions) into 20 quantiles according to their RT (Fig. 3D), and tested the RT-bin effect on the neural activity using a time-resolved 1-way repeated measures ANOVA (See Fig. 3E-F for results and examples of individual contacts). Because RT is defined as the time from target

onset to the response, the procedure sorted the response-locked trials according to target onset, and thus could unveil visual modulation of response-locked activity. The onset of the response-locked activity was modulated by target onset only in the Early Visual (120-100ms pre-response; all $p<0.04$) and the Early Caudal TPJ-Prefrontal clusters (700-680ms, 520-500ms, 300-200ms pre-response; all $p<0.004$). In the Late Caudal TPJ-Prefrontal and Late Rostral TPJ-Prefrontal clusters, the response-locked activity peak was aligned to the response without significant visual modulation. The visual modulation of response-locked activity in the Early visual and Early Caudal TPJ-Prefrontal was confirmed by a cross-correlation analysis (Fig. S5), which revealed that only for contralateral targets in these clusters the temporal dynamics of neural activity was shifted according to target-onset and this shift correlated with RT. Thus, only the clusters with early response-locked activity showed visual modulation, while later activity clusters were only sensitive to the timing of the motor response.

Finally, we examined the spatiotemporal relationships between the clusters. The three target-locked clusters formed a temporal gradient (an axis of variance in cortical features, along which areas fall in a spatially continuous order; Fig. 4A-B). The first activity cluster was the Visual cluster, which peaked around 182±78ms post-target. Then followed the Caudal TPJ-Prefrontal cluster (262±75ms post-target), and eventually the Rostral TPJ-Prefrontal cluster (383±141ms post-target) (Mixed Anova: Cluster main effect $F(2,229)=102.7$, $p<0.001$, $\eta^2=0.378$; linear polynomial contrast: $p\leq0.001$). This temporal gradient was mirrored by a topographic core-periphery gradient: a large-scale cortical organization based on the differentiation of connectivity patterns that captures a spatial and functional spectrum from perception and action (periphery) to more abstract cognitive functions (core) (*17*). The core-periphery gradient is captured by two main components: Gradient 1 extends between primary sensorimotor and transmodal regions and Gradient 2 separates somatomotor and auditory cortex from visual cortex (*17*). The Visual cluster contacts were the most peripheral and close to the visual end of Gradient 2; contacts in the Rostral TPJ-Prefrontal cluster were the closest to the core, extending from the somatomotor end to transmodal regions (Gradient 1: 1-way Anova: $F(2,229)=7.74$; $p<0.001$, $\eta^2=0.06$; linear polynomial contrast: $p\leq0.001$; Gradient 2: 1-way Anova: $F(2,229)=77.79$; $p<0.001$, $\eta^2=0.28$; linear polynomial contrast: $p\leq0.001$; Fig. 4C-D). A similar spatiotemporal gradient occurred in the response-locked clusters (Fig. 4E-H). Notably, locking activity to the response allowed teasing apart the peripheral Early Caudal TPJ-Prefrontal contacts from the Late Caudal TPJ-Prefrontal contacts, which were closer to the core.

In this study, we demonstrate that neural activity related to exogenous attention follows a spatiotemporal gradient of clusters, extending from cortical periphery to core regions, and progresses from visual to response-associated processing. The neural activity in the Caudal TPJ-prefrontal cluster, located midway along the gradient, is sensitive to spatial position and to cue-target delay, and shows IOR-dependent onset and offset. Both visual processing of the target and manual response preparation shape the neural activity in this cluster. This cluster covers a subpart of known attention networks (*18*). Our result suggest that it represents a key processing stage at the nexus between perception and action. The Rostral TPJ-Prefrontal cluster may instead encode aspects of the response: its neural activity shows sensitivity to the stimulus identity (stronger responses to targets than to cues). Additional elements that link this cluster to response-related processes are its lateralization to the left hemisphere, contralateral to the responding hand, the fact that its target-locked activity is modulated by the response, and the peak of its response-locked activity at the time of the motor response. Furthermore, this cluster is anatomically situated between the somatomotor end and transmodal core regions of the core-periphery gradients.

The Caudal TPJ-prefrontal and Rostral TPJ-prefrontal clusters overlap with known frontoparietal attention networks (*18–20*), but the distinct portions of the TPJ they occupy differ in their functional and structural connectivity (*21–24*). The middle branch of the superior longitudinal fasciculus (SLF II) connects the caudal TPJ, a part of the right-lateralized ventral attention network, with the superior frontal gyrus/FEF of the dorsal attention network (*21*, *23*, *24*), thus providing direct communication between the ventral and dorsal attention networks. The degree of SLF II right lateralization correlates with physiological leftwards spatial bias (*21*). Transitory inactivation of the SLF II during brain surgery provoked severe signs of left spatial neglect (*25*). Consistent with these findings, the Caudal TPJ-prefrontal cluster in our data was lateralized to the right hemisphere. The ventral branch of the SLF (SLF III) connects the rostral part of the TPJ with the middle and inferior frontal gyri, thus connecting nodes of the ventral attention network. It is lateralized to the right hemisphere (*21*) and was shown to be disconnected in patients suffering from visual neglect who present abnormal IOR in their ipsilesional visual field (*12*). Therefore, these two clusters appear to represent two distinct frontoparietal networks implicated in exogenous attention.

The clusters we identified form a perception-attention-response continuum along the periphery-core cortical gradient. The gradient spans between sensorimotor and transmodal areas, and is suggested to be a primary organizing axis of the human cerebral cortex (*17*, *26*). The position of a cortical region along this gradient reflects its microstructural and genetic features, connectivity profile, and functional role (*26*, *27*). The Visual cluster is situated at the peripheral end of the cortical gradient; its neural responses to the cue and target were segregated, even at the short cue-target delay. Conversely, the Caudal TPJ-Prefrontal and the Rostral TPJ-Prefrontal clusters were located closer to core regions of the cortical gradient, and their cue and target neural responses at the short cue-target delay were integrated in a single peak of activity. This phenomenon is consistent with a key feature of the core-periphery gradient: a temporal hierarchy of receptive windows, analogous to the spatial hierarchy of receptive fields (*26–32*). Going from peripheral regions such as early visual cortex, to core regions such as the intraparietal sulcus, temporal receptive windows become longer, integrating over longer durations, and selectivity for coherent temporal structures increases (*26*, *28–30*). Such hierarchy of temporal scales could serve the agent's dynamical interaction with a continuously changing environment, from fast fluctuations associated with sensory processing at the bottom of the hierarchy, to slow contextual changes in the environment at its the highest levels, under which faster representations unfold (*29*). Recurrent temporal computations along the temporal hierarchy could help incorporating prior events, by increasing selectivity to temporal patterns and enhancing robustness to noise (*30*).

Our results reveal temporal operations at the basis of the psychological concept of exogenous attention. They are consistent with the hypothesis that *RT facilitation* results from a summation of cue-related and target-related responses, thus reflecting hard-wired limitations of the neural system that cannot respond separately to rapidly repeated stimuli, and processes them as a single event (*1*, *33*, *34*). Longer cue-target delays could instead provide the system with enough time to segregate cue- and target-related responses (*1*, *33*). The integration of cue-target responses in the Caudal TPJ-Prefrontal and the Rostral TPJ-Prefrontal clusters in the long-SOA could result from temporal pooling, i.e. the integration of prior information across the temporal window that makes neural response robust to changes in the precise timing of inputs (*30*). In the Visual cluster, situated lower in the hierarchy, temporal receptive windows are shorter, thus cue-induced activity is segregated from the target-induced activity even at short cue-target delays. During further processing in frontoparietal clusters, cue- and target-induced activities resulted in a single activity peak. This temporal pooling might group the cue and target in a single event (*34*), leading to *RT facilitation* at short cue-target delays (*1*, *33*, *34*). Over longer cue-target delays, which allowed temporal segregation

of cue and target, IOR could result from temporal normalization, an operation that leads to decreased response to repeating stimuli and increased response to novel ones (*30*–*32*). Recent evidence (*27*) shows that neural timescales can change to serve cognitive functions. Specifically, prefrontal cortex timescales expand during working memory maintenance and predict individual performance (*27*).

Our results offer a model of time-resolved segregation and integration of visual events across a gradient of cortical processing streams, and uncover the fine-grained spatiotemporal characteristics of the neural processes underlying exogenous attention in the human brain.

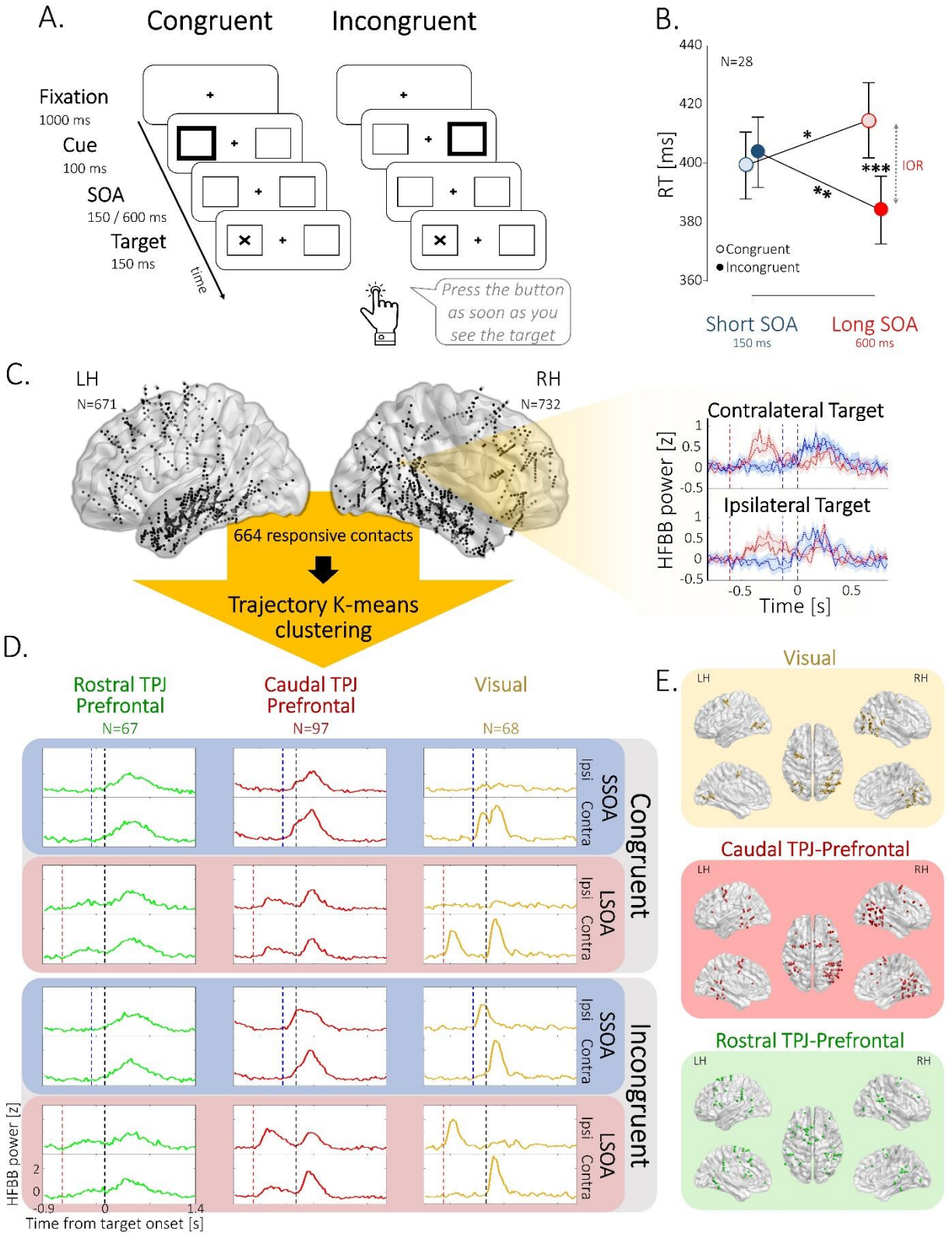

Figure 1 - Neurotypical performance of implanted patients in the Posner task, contact localization and trajectory clustering. A. Illustration of the Posner cued detection task. After 1000ms of fixation, a cue (thickened placeholder) appeared for 100ms at either side of the screen. On short SOA trials (SSOA), the target ('X') occurred 150ms after cue onset; on long SOA trials (LSOA) the target appeared 600ms after cue onset. The target appeared either on the same side of the screen as the Cue (Congruent

condition), or on the opposite site (Incongruent condition). Patients were required to press a central button with their right hand, as soon as the target appeared, while maintaining central fixation throughout stimuli presentation. Catch trials (n=24) had the same duration and cue presentation, but no target followed the cue. All trial types (n=336) were equiprobable and randomly interleaved. Stimuli are not drawn to scale. B. Patients' performance is neurotypical. * p=0.047; ** p=0.008; *** p<0.001. Error bars represent normalized SEM. C. Left panel: Illustration of the localization of the contacts included in the analysis (black circles; N=1,403) in the left hemisphere (LH; N=671) and in the right hemisphere (RH, N=732), pooled across all patients. Each localization is the mean coordinates of the two contacts composing the contact's bipolar montage, depicted in normalized space (MNI152) for visualization. All included contacts were in grey matter or its immediate proximity. To reveal prototypical temporal patterns simultaneously across all conditions, the trajectories across the 8 condition dimensions of the mean high-frequency broadband (HFBB) target-locked activity of 664 significantly responsive contacts (significant time-point-by-time-point t-test for at least 100ms in one of the experimental conditions compared to baseline), were clustered using a novel trajectory K-means clustering approach. Right panel: Example of target-locked mean normalized HFBB responses of one contact in the right angular gyrus in Congruent (full lines) and Incongruent (dashed lines) trials, at short-SOA (blue) and long-SOA (red), with targets contralateral or ipsilateral to the contact. Dashed vertical lines represent target onset (black) and cue onset at short-SOA (blue) and long-SOA (red). Shaded areas represent SEM across trials for each sample. D. Prototypical temporal profiles of contact clusters showing dynamic activity across experimental conditions: Trimmed-mean target-locked activity profiles of three contact clusters, across the 8 conditions (Congruent / Incongruent Trial X short-SOA / long-SOA X Ipsilateral target (Ipsi) / contralateral target (Contra)). Visual cluster (yellow) shows contralateral fast responses, with cue-target activity segregation at both SOAs; Caudal TPJ-Prefrontal cluster (red) shows bilateral slower responses with spatial sensitivity, with cue-target activity segregation at long-SOA but response integration in SSOA; and Rostral TPJ-Prefrontal cluster (green) shows bilateral slower responses with stimulus type sensitivity, with cue-target activity segregation at long-SOA but response integration at SSOA. Dashed vertical lines represent target onset (black) and cue onset at short-SOA (blue) and long-SOA (red). E. Clusters' spatial profile. Illustration of the localization of the contacts composing each cluster: Visual cluster (yellow), Caudal TPJ-Prefrontal cluster (red), Rostral TPJ-Prefrontal cluster (green). For each cluster, dots represent contacts' localization in dorsal (middle), lateral (top) and medial (bottom) views of the right hemisphere (RH; right) and of the left hemisphere (LH; left).

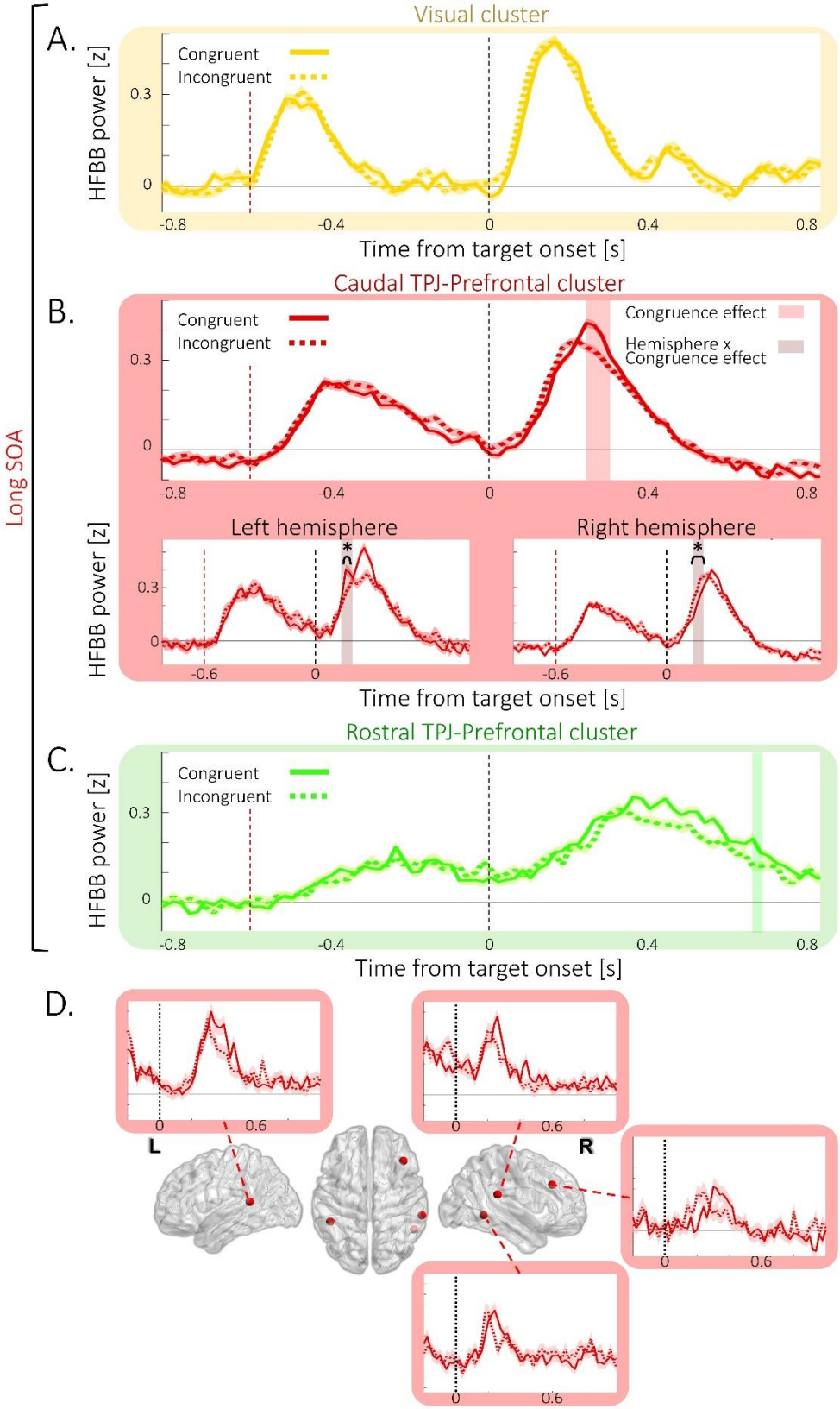

Figure 2 - IOR-related neural activity. Mean target-locked long-SOA activity in the Visual (yellow), Caudal TPJ-Prefrontal (red) and Rostral TPJ-Prefrontal (green) clusters, computed over trials of contacts, for Congruent trials (full lines) and Incongruent trials

(dashed lines). A. In the Visual cluster, no significant Congruence effect was observed. B. In the Caudal TPJ – Prefrontal cluster activity in Congruent and Incongruent trials (IOR-related) differed significantly at 0.24-0.3s post target (shaded red areas; Congruence main effect: all $p_{corrected}$horizontal$_d$<0.002), and a significant hemispheric difference between IOR-related responses was observed at 0.14-.022s post target (shaded brown area; Hemisphere x Congruence interaction: all $p_{corrected}$<0.03). C. In the Rostral TPJ – Prefrontal cluster activity in Congruent and Incongruent trials differed significantly at 0.66-0.68s post target (green shaded area; Congruence main effect: all $p_{corrected}$<0.003). A-C. Shaded areas around traces depict SEM; Dashed vertical lines represent Target onset (black) and Cue onset (red) at the long-SOA condition; asterisks represent significant Congruence x Hemisphere post hoc comparisons ($p_{corrected}$<0.05). D. Representative examples of HFBB power IOR-related activity in the Congruent (full line) & Incongruent (dashed line) long-SOA conditions of individual contacts of the Caudal TPJ-Prefrontal cluster.

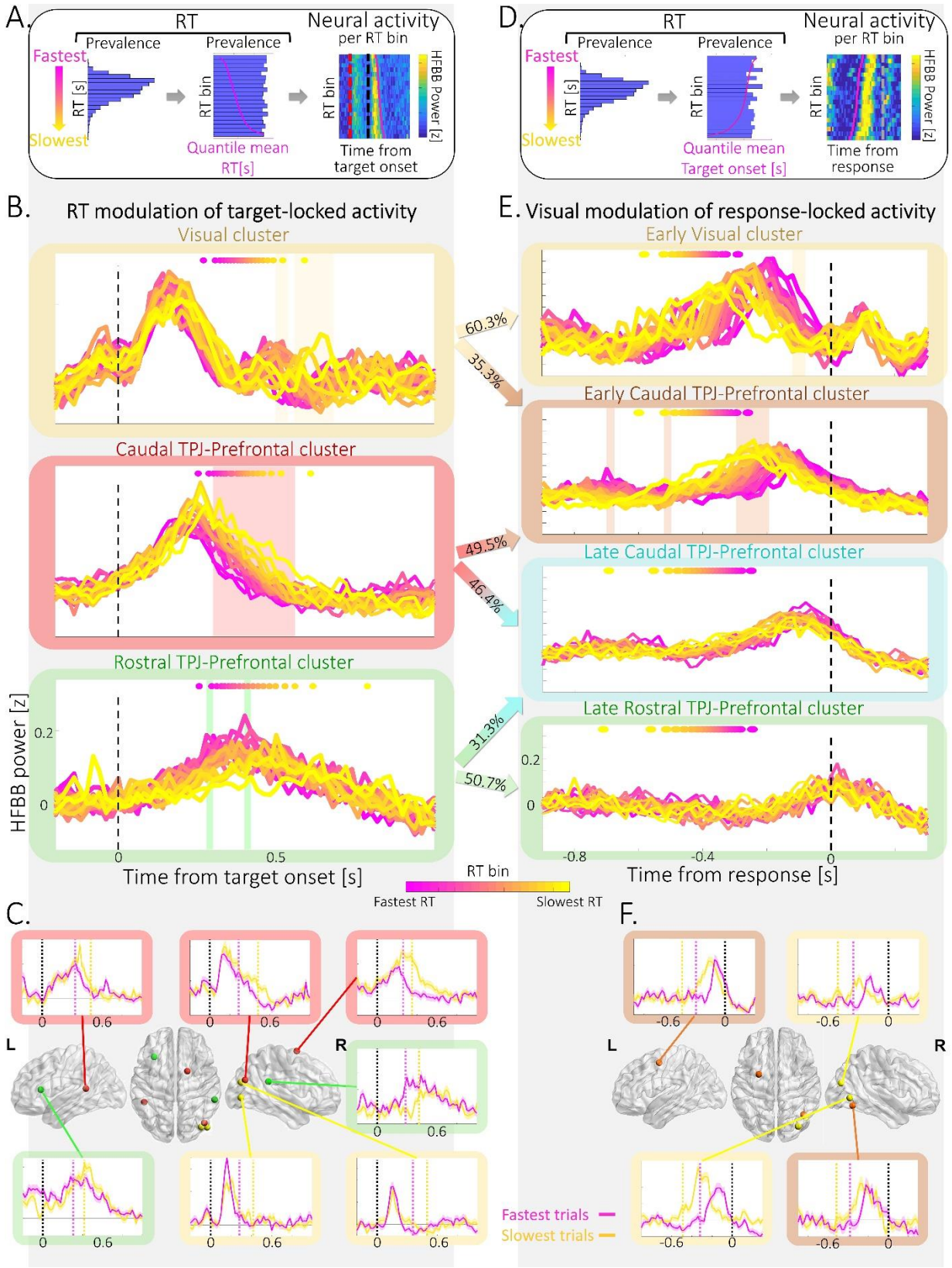
A.
RT
Neural activity
per RT bin
Prevalence
Prevalence
Fastest
Slowest
RT [s]
RT bin
RT bin
HFBB Power [z]
Quantile mean
RT[s]
Time from
target onset
D.
RT
Neural activity
per RT bin
Prevalence
Prevalence
Fastest
Slowest
RT [s]
RT bin
RT bin
HFBB Power [z]
Quantile mean
Target onset [s]
Time from
response
B.
RT modulation of target-locked activity
Visual cluster
Caudal TPJ-Prefrontal cluster
Rostral TPJ-Prefrontal cluster
HFBB power [z]
0.2
0
0
0.5
Time from target onset [s]
E.
Visual modulation of response-locked activity
Early Visual cluster
Early Caudal TPJ-Prefrontal cluster
Late Caudal TPJ-Prefrontal cluster
Late Rostral TPJ-Prefrontal cluster
60.3%
35.3%
49.5%
46.4%
31.3%
50.7%
0.2
0
-0.8
-0.4
0
Time from response [s]
RT bin
Fastest RT
Slowest RT
C.
L
R
0
0.6
F.
L
R
-0.6
0
Fastest trials
Slowest trials

Figure 3 - RT & visual modulation of Target-locked & Response-locked Neural activity. A. Schematic illustration of the procedure for computing neural activity at different RT bins: Within each cluster, the trial distribution of RTs (left) was divided into 20 quantiles (RT bins; middle). RT bins were ordered according to their mean RT (magenta line), and the quantile's mean target-locked neural activity pooled across cluster contacts, was computed (right). B. RT modulates target-locked neural activity. Top: Late RT modulation of activity in the Visual cluster (yellow): Main effect of RT bin was observed at 0.5-0.54 & 0.56-0.68s post target onset (shaded yellow area; all $p_{corrected}$<0.002), suggesting RT-related late modulation after response offset & button press time. Middle: RT modulation of neural response offset and button press time in Caudal TPJ – Prefrontal cluster (red): Main effect of RT bin was observed at 0.3-0.56s post target onset (shaded red area; all $p_{corrected}$<0.028), suggesting RT modulation of response offset. Bottom: RT modulation of response in Rostral TPJ – Prefrontal cluster (green): Main effect of RT bin occurred at 0.28-0.3 and0.4-0.42s post target onset (shaded green area; all $p_{corrected}$<0.007), suggesting RT modulation around neural response peak and button-press time. RT modulation of clusters' target-locked activity (pooled across conditions; yellow: Slowest RT bin; Magenta: fastest RT bin; Dashed vertical lines represent Target onset (black) and Cue onset at the short-SOA (blue) and long-SOA (red) conditions); Color-coded dots at the top represent mean RT for each RT bin (pink – fastest RT to yellow – slowest RT). C. Typical examples of HFBB power activity of the fastest (pink) & slowest (yellow) third of all trials of single contacts of the three target-locked clusters. D. Schematic illustration of the procedure for computing neural response-locked activity at different RT bins: Within each cluster, the trial distribution of RTs in each condition (left) was divided into 20 quantiles (RT bins; middle). RT bins were ordered according to their mean RT. Since RT is defined as the interval between target onset and the response, the quantile's mean RT corresponds here to target onset time (magenta line). Then, each quantile's mean response-locked neural activity pooled across all cluster contacts was computed (right). Grey dashed line denotes motor response time. E. Top: Target onset time modulates activity in the Early visual cluster (yellow): Main effect of RT-bin was observed at 0.12-0.10s pre-response (shaded yellow area; all $p_{corrected}$<0.04). Target onset time modulates activity in Rostral Visual-Prefrontal cluster (orange): Main effect of RT bin was observed at 0.70-0.68s, 0.52-0.50s & 0.30-0.20s pre-response (shaded orange area; all $p_{corrected}$<0.004). No significant modulation of activity in Late Caudal TPJ-Prefrontal (turquoise) & Late Rostral TPJ-Prefrontal (green) clusters by target onset time. E. Representative examples of HFBB power activity of the fastest (pink) & slowest (yellow) third of all trials of individual contacts of the Early Visual and Early Caudal TPJ-Prefrontal clusters.

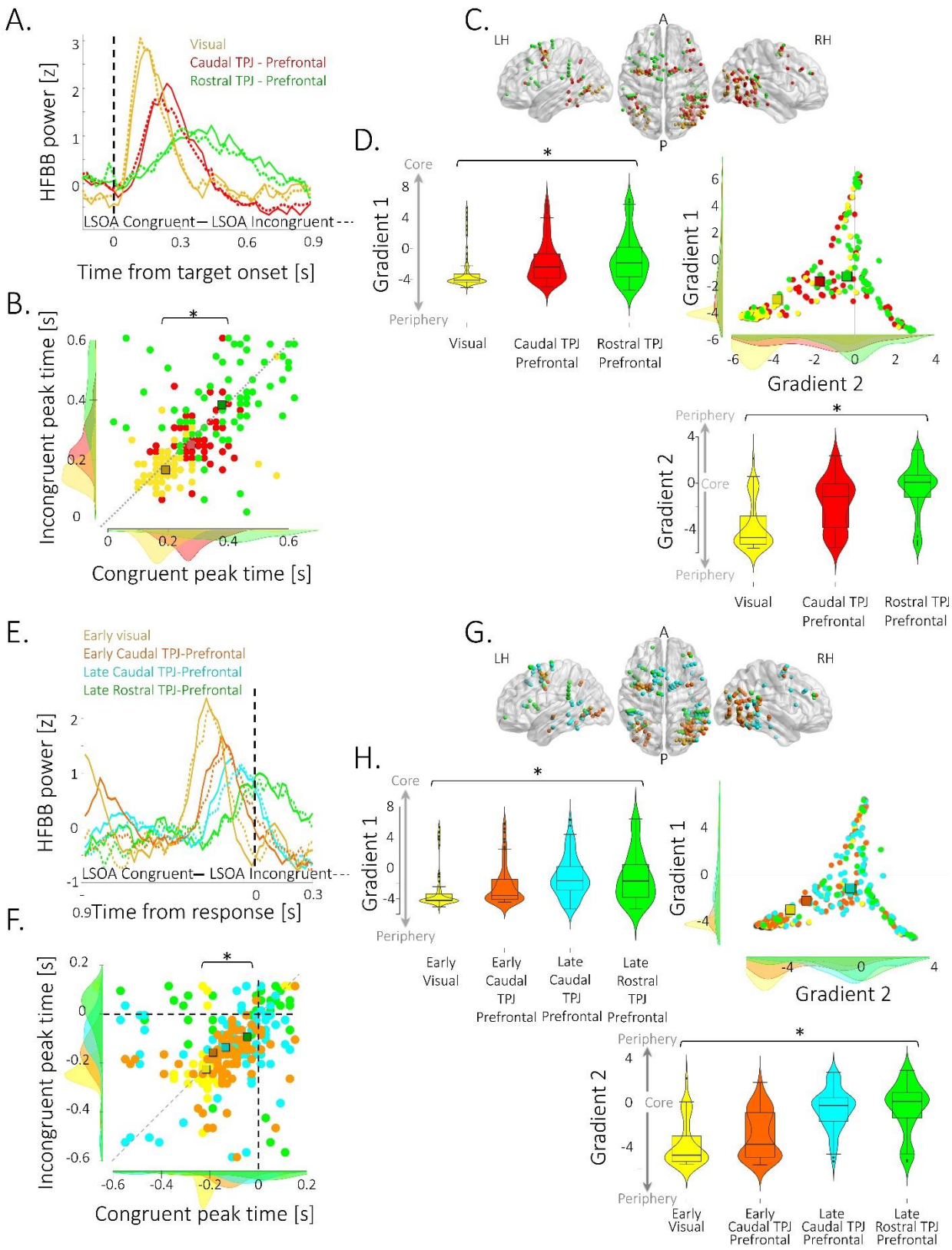

Figure 4 – Clusters exhibit a spatiotemporal gradient. A. Temporal gradient of activity in target-locked clusters: Trimmed-mean target-locked response of the Visual cluster, Caudal TPJ-Prefrontal and Rostral TPJ-Prefrontal clusters. Black dashed line depicts

target onset. B. Scatter plot of peak times of mean target-locked activity of the contacts of the Visual (yellow circles), the Caudal TPJ-Prefrontal (red circles) and the Rostral TPJ-Prefrontal (green circles) clusters, in the Congruent (x axis) and Incongruent (y-axis) conditions, showing a significant temporal gradient ($p<0.001$, $\eta^2=0.378$; linear polynomial contrast: $p\leq0.001$). Squares represent mean peak time; Dotted grey line denotes the equity line; Shaded areas represent peak time distributions. C. Core-Periphery gradient: Clusters' anatomical localization follows Core-Periphery gradients (17), where Visual cluster's contacts are the most peripheral and Rostral TPJ-Prefrontal cluster's contacts are closest to core regions. D. Top left and bottom right: Box plots of contacts localization along Core-Periphery gradients for the Visual (yellow), the Caudal TPJ-Prefrontal (red) and the Rostral TPJ-Prefrontal (green) clusters, showing a significant core-periphery gradient (Gradient 1: $p<0.001$, $\eta^2=0.06$; linear polynomial contrast: $p\leq0.001$; Gradient 2: $p<0.001$, $\eta^2=0.28$; linear polynomial contrast: $p\leq0.001$). Middle: Scatter plot of contacts localization along core-periphery gradients (Visual cluster - yellow circles; Caudal TPJ-Prefrontal cluster - red circles; Rostral TPJ-Prefrontal – green circles). E. Temporal gradient of activity in response-locked clusters: Trimmed-mean response-locked response of the Early Visual cluster, Early Caudal TPJ-Prefrontal and Late Caudal TPJ-Prefrontal and Late Rostral TPJ-Prefrontal clusters. Black dashed line depicts RT. F. Scatter plot of peak times of mean response-locked activity of the contacts of the Early Visual (yellow circles), the Early Caudal TPJ-Prefrontal (orange circles), the Late Caudal TPJ-Prefrontal (turquoise circles) and the Late Rostral TPJ – Prefrontal (green circles) clusters, in the Congruent (x axis) and Incongruent (y-axis) long-SOA conditions, showing a significant temporal gradient ($p<0.001$, $\eta^2=0.086$; linear polynomial contrast: $p\leq0.001$). Squares represent mean peak time; Dotted grey line denotes the equity line; Shaded areas represent peak time distributions. G. Core-Periphery gradient: Clusters' anatomical localization follows Core-Periphery gradients (17), where Early Visual cluster's contacts are the most peripheral and Late Rostral TPJ-Prefrontal cluster's contacts are closest to core regions. H. Top left & bottom right: Box plots of contacts localization along Core-Periphery gradients for the Early Visual (yellow), the Early Caudal TPJ-Prefrontal (orange), the Late Caudal TPJ-Prefrontal (turquoise) and the Late Rostral TPJ-Prefrontal (green) clusters, showing a significant core-periphery gradient (Gradient 1: $p=0.001$, $\eta^2=0.06$; linear polynomial contrast: $p\leq0.001$; Gradient 2: $p<0.001$, $\eta^2=0.32$; linear polynomial contrast: $p\leq0.001$). Middle: Scatter plot of contacts localization along core-periphery gradients (Visual cluster - yellow circles; Caudal TPJ-Prefrontal cluster - red circles; Rostral TPJ-Prefrontal cluster - green circles).

Patient #	Age	Gender	Handedness	Number of electrodes (total 243)	Total number of contacts (total 1,884)	Implanted hemisphere
1	49	M	R	10	104	RH
2	44	F	R	12	96	LH+RH
3	31	M	R	12	82	RH
4	31	F	R	10	82	LH
5	26	M	R	9	58	RH
6	47	M	R	11	90	LH
7	31	F	R	9	54	LH
8	30	M	R	9	63	LH
9	26	M	L+R	10	44	LH+RH
10	24	M	R	9	48	LH
11	26	F	R	10	88	LH
12	22	F	R	10	58	RH
13	34	F	R	8	76	LH
14	40	F	R	7	62	LH
15	34	M	R	10	70	LH+RH
16	45	F	R	9	78	LH+RH
17	24	F	R	8	61	RH
18	19	M	R	7	65	RH
19	34	M	R	7	31	RH
20	47	M	R	8	53	LH
21	31	F	L	8	56	LH
22	31	M	L	5	48	LH
23	26	F	R	8	63	RH
24	26	F	R	9	77	RH
25	31	F	R	9	67	LH+RH
26	21	F	R	9	54	LH+RH
27	30	F	R	12	93	RH
28	28	M	R	11	62	LH
Mean	**31.7±8.1**	**54% F**	**89% R**	**9.1**	**67.3**	**57% RH**

Table 1 – Implanted patients demographic details

Region name	Responsive Electrodes N	Visual cluster N	Caudal TPJ-Prefrontal cluster N	Rostral TPJ-Prefrontal cluster N
Banks superior temporal sulcus	9	1	4	1
Caudal anterior-cingulate cortex	3	0	0	0
Caudal middle frontal gyrus	12	2	2	1
Entorhinal cortex	6	0	0	0
Fusiform gyrus Posterior	33	7	8	3
Fusiform gyrus Med	14	2	2	0
Fusiform gyrus Anterior	10	0	0	0
Inferior parietal cortex	51	19	14	5
Inferior temporal gyrus Posterior	28	1	8	1
Inferior temporal gyrus Middle	14	0	3	0
Inferior temporal gyrus Antrior	13	0	0	0
Lateral occipital cortex	20	6	5	2
Lingual gyrus	17	1	0	3
Medial orbital frontal cortex	4	0	0	0
Middle temporal gyrus Posterior	37	10	12	1
Middle temporal gyrus Middle	19	0	2	0
Middle temporal gyrus Anterior	35	0	0	0
Parahippocampal gyrus	8	0	0	0
Paracentral lobule	1	0	0	0
Pars opercularis	8	0	0	1
Pars orbitalis	36	0	0	0
Pars triangularis	9	0	0	4
Pericalcarine cortex	1	0	0	0
Postcentral gyrus dorsal	1	0	0	0
Postcentral gyrus ventral	1	0	0	0
Posterior-cingulate cortex	3	0	1	1
Precentral gyrus dorsal	16	6	3	4
Precentral gyrus ventral	5	0	3	1
Precuneus cortex	1	0	0	0
Rostral middle frontal gyrus	16	0	4	2
Superior frontal gyrus	46	0	8	16
Superior parietal cortex	10	1	3	1
Superior temporal gyrus Posterior	19	2	1	3
Superior temporal gyrus Middle	17	0	0	0
Superior temporal gyrus Anterior	13	0	0	3
Supramarginal gyrus	22	0	3	9
Temporal pole	14	0	0	0
White matter	49	10	10	5
hippocampus	18	0	1	0
amygdala	5	0	0	0

Table 2 – Responsive electrodes localization according to the Desikan-Killiany-Tourville atlas (35)

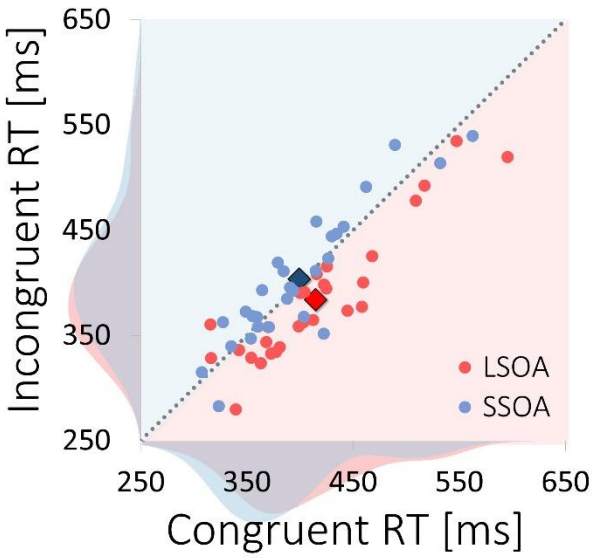

Figure S1- *Individual RT effects. A scatter plot of patients' RT, showing each patient's Congruent trials' RT (X axis) and Incongruent trials' RT (y axis), in the Long SOA condition (LSOA; red dots) and in the Short SOA condition (SSOA; blue dots). Squares represent group mean RT. Dotted line denotes the equity line, samples below it demonstrate IOR (shaded red), and samples above it demonstrate RT facilitation (shaded blue). RT distributions for long-SOA (shaded red) and short-SOA (shaded blue) conditions, for congruent trials (x-axis) and Incongruent trials (y-axis).*

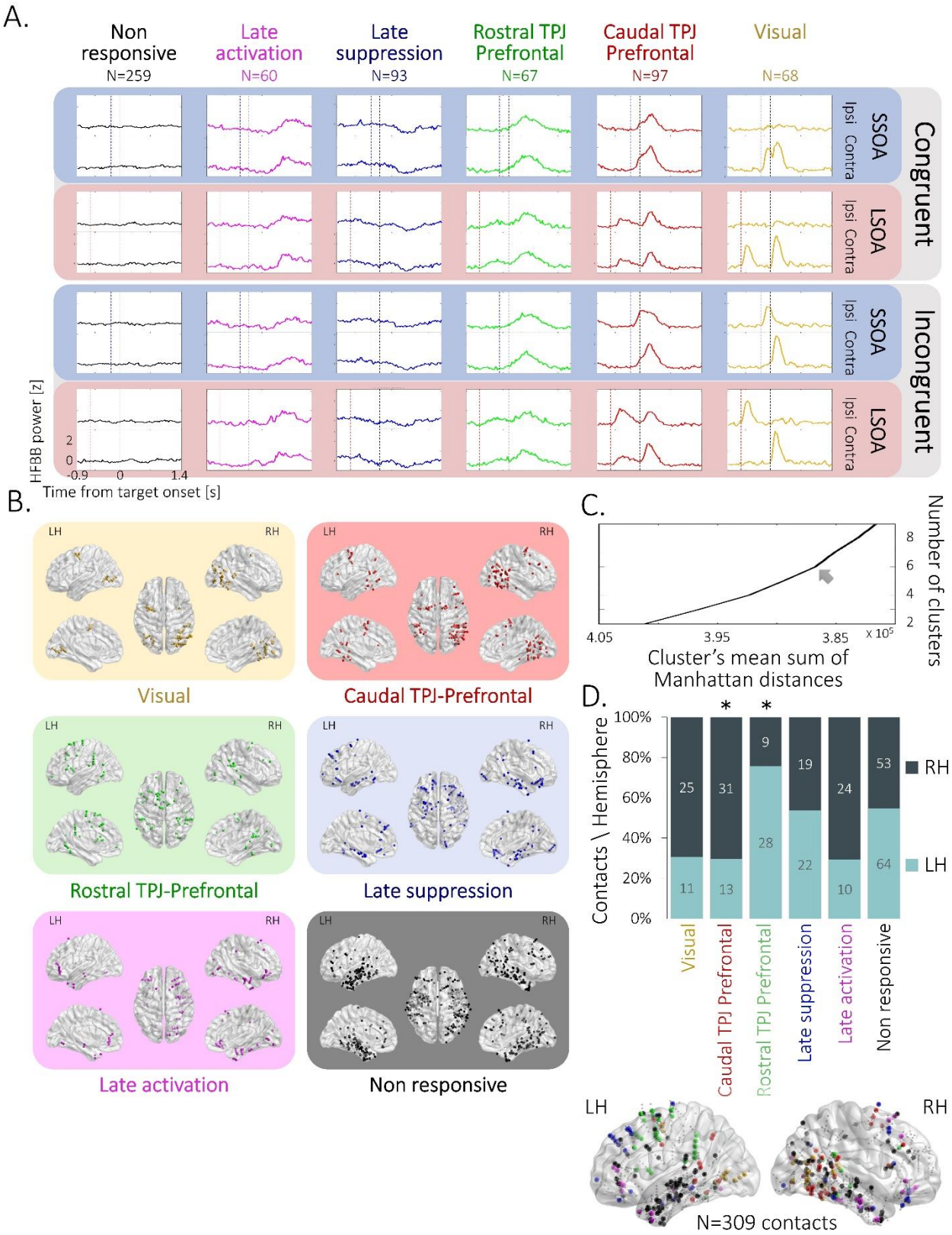

Figure S2 – *Clusters' spatiotemporal profile. A. Prototypical activity profiles of contact clusters: Trimmed-mean target-locked activity profiles of the six contact clusters: Visual cluster (yellow); Caudal TPJ-Prefrontal cluster (red); Rostral TPJ-Prefrontal cluster*

(green); Late suppression cluster (blue); Late activation cluster (magenta); Non responsive cluster (black), across the 8 conditions (Congruent / Incongruent X short-SOA / long-SOA X Ipsilateral target (Ipsi) / contralateral target (Contra)). Dashed vertical lines represent Target onset (black) and Cue onset at short-SOA (blue) and long-SOA (red) conditions. B. Clusters' spatial profile. Illustration of the localization of the contacts composing each cluster: Visual cluster (yellow); Caudal TPJ-Prefrontal cluster (red); Rostral TPJ-Prefrontal cluster (green); Late suppression cluster (blue); Late activation cluster (magenta); Non responsive cluster (black). For each cluster, dots represent contacts' localization, computed as the mean coordinates of the two contacts composing each contact's bipolar montage, depicted in normalized space (MNI152) in dorsal (middle), lateral (top) and medial (bottom) views in the right hemisphere (RH; right) and the left hemisphere (LH; left). C. Elbow method. Mean sum of Manhattan distances between each contact trajectory and its assign cluster trajectory for 2-9 clusters' solution. Maximal elbow (grey arrow) is observed at the 6-cluster solution. Clusters' hemispheric lateralization. D. Clusters' spatial distribution in symmetrically covered regions significantly differs between right and left hemispheres (dark grey & light grey respectively; $X^2_{(5)}=29.09$, $p<0.001$), resulting from a significant right lateralization of Caudal TPJ-Prefrontal cluster (red) and a significant left lateralization of Rostral TPJ-Prefrontal cluster (green; post hoc binomial tests, $p=0.01$ and $p<0.003$). Symmetrically covered regions were defined by calculating the overlap between the volumes of 3mm radius spheres around each contact for each hemisphere (see methods). Proportion of colors in each bar represent the percentage of contacts per hemisphere in each cluster; numbers are raw contact number per hemisphere in each cluster.

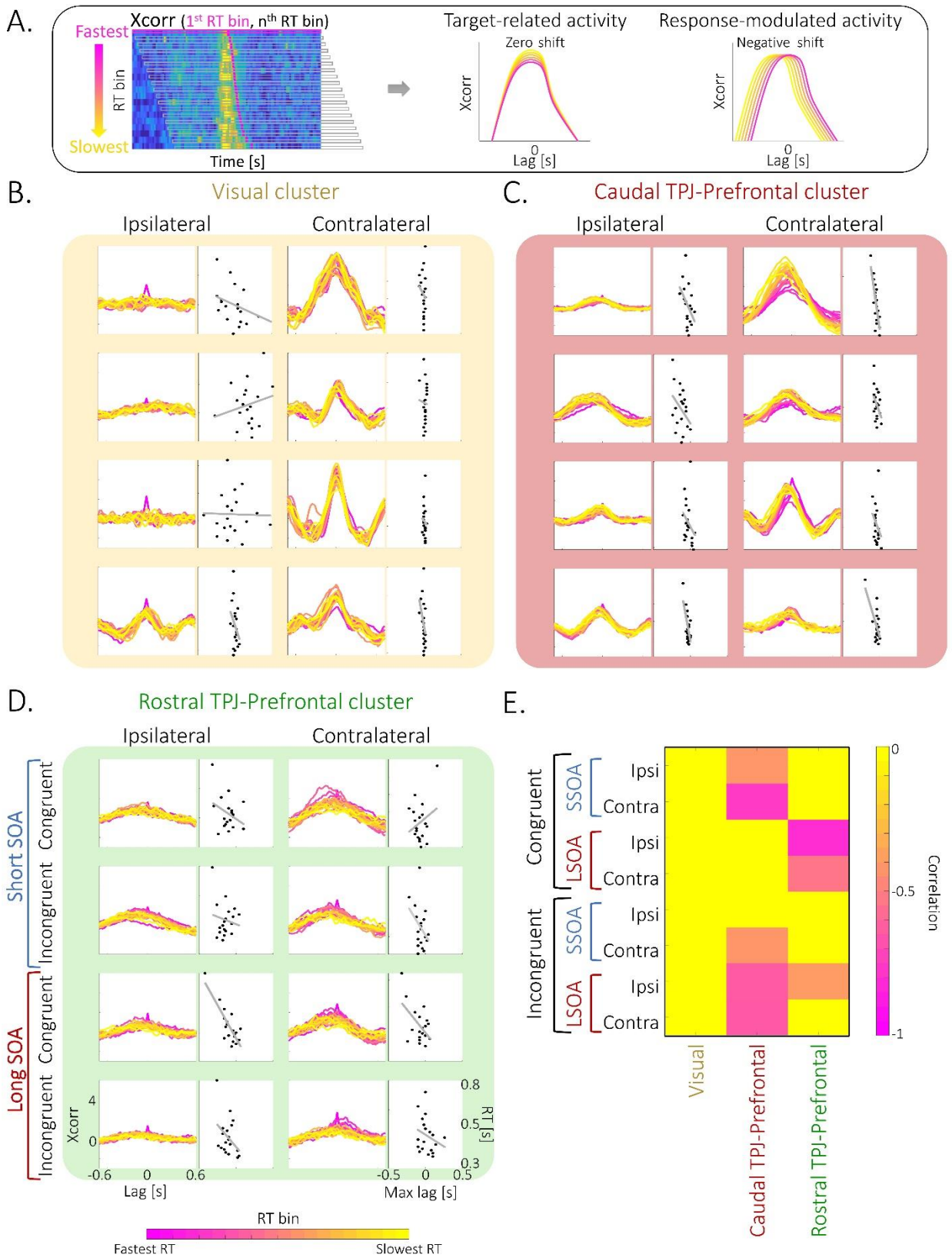
A.
Xcorr (1st RT bin, nth RT bin)
Fastest
RT bin
Slowest
Time [s]
Target-related activity
Zero shift
Xcorr
0
Lag [s]
Response-modulated activity
Negative shift
Xcorr
0
Lag [s]
B.
Visual cluster
Ipsilateral
Contralateral
C.
Caudal TPJ-Prefrontal cluster
Ipsilateral
Contralateral
D.
Rostral TPJ-Prefrontal cluster
Ipsilateral
Contralateral
Short SOA
Congruent
Incongruent
Long SOA
Congruent
Incongruent
Xcorr
4
0
-0.6
0
0.6
Lag [s]
-0.5
0
0.5
Max lag [s]
RT [s]
0.8
0.5
0.3
RT bin
Fastest RT
Slowest RT
E.
Congruent
SSOA
Ipsi
Contra
LSOA
Ipsi
Contra
Incongruent
SSOA
Ipsi
Contra
LSOA
Ipsi
Contra
Visual
Caudal TPJ-Prefrontal
Rostral TPJ-Prefrontal
Correlation
0
-0.5
-1

Figure S3 –Cluster neural target-locked activity timing is correlated with behavior. A. Schematic illustration of the procedure for computing the cross-correlation (Xcorr) between neural activity across RT bins: Cross-correlation between target-locked activity at the fastest RT bin and all subsequent bins was computed (left). If cluster activity is response-associated, maximal cross-correlation will follow the RT, resulting in a negative shift of cross-correlation lag (middle). If cluster activity is target-associated, maximal cross-correlation will be centered around target onset, resulting in a zero shift across all RT bins (right). B.-D. Cross-correlogram of neural activity at different RT bins (pink- fastest RT; yellow - slowest RT) as a function of cross-correlation lag (left columns) and Pearson correlation (grey line) between maximal cross-correlation lags (Max lag) and bin's mean RTs (right columns), across the 8 conditions (Congruent / Incongruent X short-SOA / long-SOA X Ipsilateral target / contralateral target) in the Visual (yellow), Caudal TPJ-Prefrontal (red) and Rostral TPJ-Prefrontal (green) clusters. B. Visual cluster activity is target-associated: Cross-correlation plots are centered around zero, especially for contralateral targets. C. Activity in the Caudal TPJ – Prefrontal cluster is response-associated: Cross-correlation plots show a negative shifted lag that is generally correlated with RT. D. Rostral TPJ – Prefrontal cluster activity is response-associated: Cross-correlation plots show a negative shifted lag, correlated with RT under certain conditions. E. Significant negative correlation between cross-correlation maximal lag and bin mean RT in the Caudal TPJ – Prefrontal & Rostral TPJ – Prefrontal clusters: significant ($p<0.05$) negative correlations were found only in these two clusters.

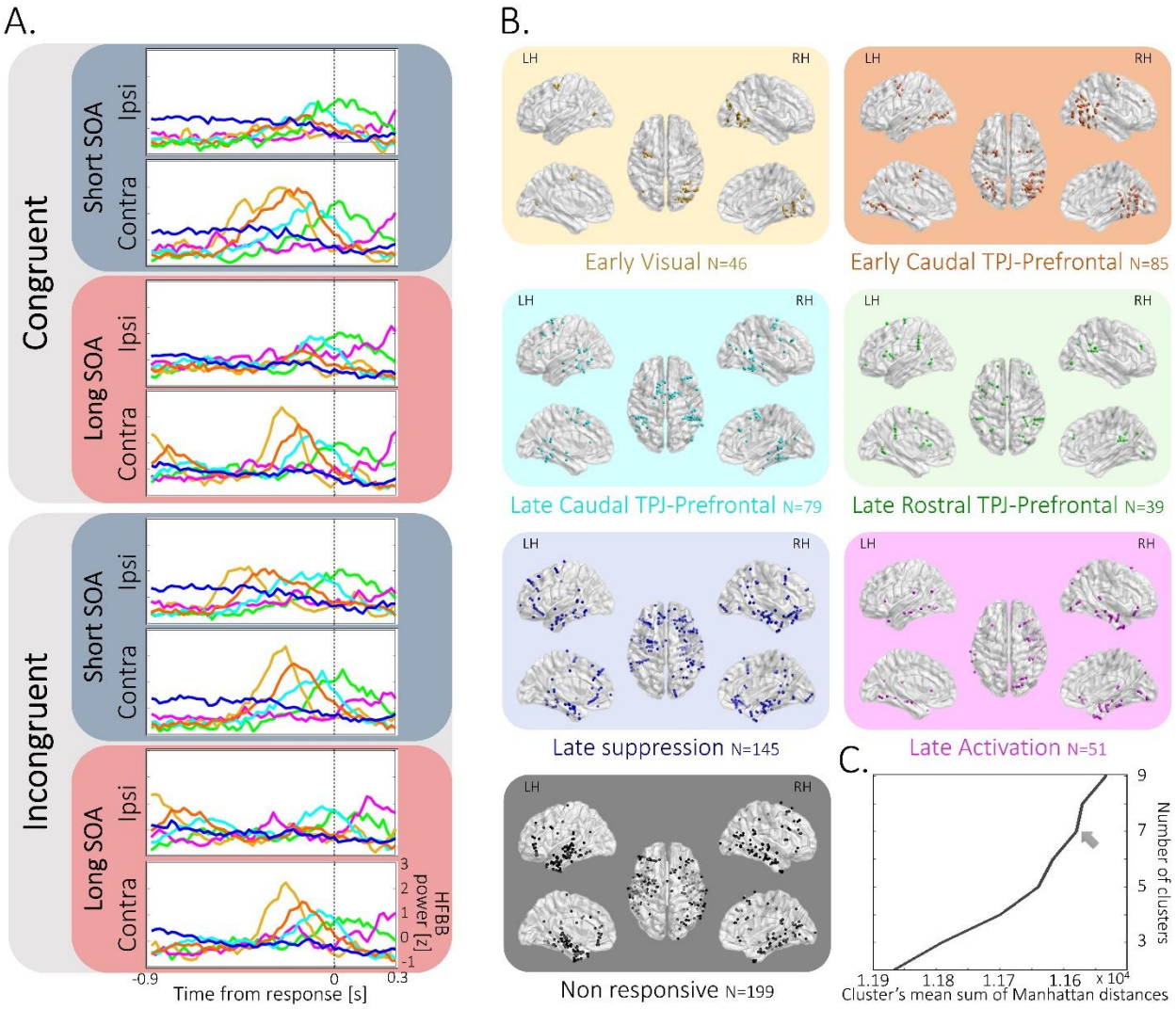

D.

Response-locked clusters

Target-locked clusters	Early Visual	Early Caudal TPJ-Prefrontal	Late Caudal TPJ-Prefrontal	Late Rostral TPJ-Prefrontal	Late suppression	Late Activation	Non responsive	
Visual	41 60.3%	24 35.3%	0 0%	0 0%	0 0%	1 1.5%	2 2.9%	68 100%
Caudal TPJ-Prefrontal	1 1%	48 49.5%	45 46.4%	1 1%	2 2.1%	0 0%	0 0%	97 100%
Rostral TPJ-Prefrontal	0 0%	4 6%	21 31.3%	34 50.7%	0 0%	5 7.5%	3 4.5%	67 100%
Late suppression	2 2.2%	0 0%	0 0%	0 0%	82 88.2%	0 0%	8 8.6%	60 100%
Late activation	1 1.7%	0 0%	0 0%	1 1.7%	14 23.3%	31 51.7%	13 21.7%	60 100%
Non responsive	1 0.4%	9 3.5%	12 4.6%	3 1.2%	47 18.1%	14 5.4%	173 66.8%	259 100%

Figure S4 – Response-locked clusters' spatiotemporal profile. A. Trimmed-mean response-locked activity profiles of the seven contact clusters across the 8 conditions (Congruent / Incongruent X short-SOA / long-SOA X Ipsilateral target / contralateral target): Early visual cluster (yellow); Early Caudal TPJ-Prefrontal cluster (orange); Late Caudal TPJ-Prefrontal cluster (turquoise); Late Rostral TPJ-Prefrontal cluster (green); Late suppression cluster (blue); Late activation cluster (magenta); Non responsive cluster (black). Dashed vertical lines represent Target onset (black) and Cue onset at short-SOA (blue) and long-SOA (red) conditions. B. Response-locked clusters' spatial location. Illustration of the localization of the contacts composing each cluster (colors as in A). For each cluster, dots represent contacts' localization, computed as the mean coordinates of the two contacts composing each contact's bipolar montage, depicted in normalized space (MNI152) in dorsal (middle), lateral (top) and medial (bottom) views in the right hemisphere (RH) and the left hemisphere (LH). C. Elbow method. Mean sum of Manhattan distances between each contact trajectory and its assigned cluster trajectory for 2-9 clusters' solution. Maximal elbow (grey arrow) is observed at 7 cluster solution. D. Contingency table showing the mapping between target-locked and response-locked clusters. The distribution of target-locked clusters' contacts (rows; number of contacts & % within row) across the different response-locked clusters (columns) was significantly different than chance ($X^2_{(30)}=1442$; $p < 0.001$; Contingency coefficient =0.83).

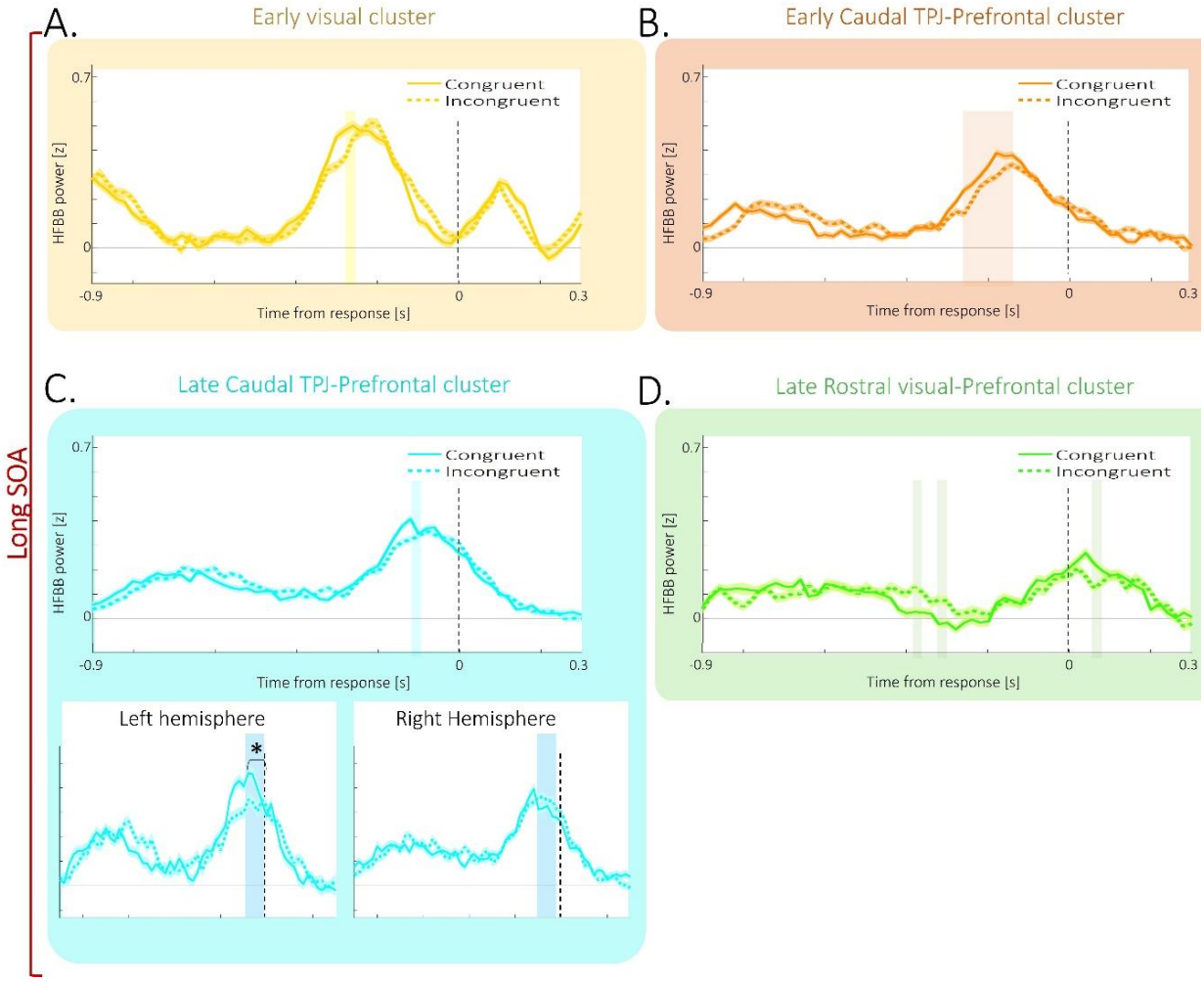

Figure S5 - IOR-related response-locked neural activity. Mean response-locked long-SOA activity in the Early Visual (yellow), Early Caudal TPJ-Prefrontal (orange), Late Caudal TPJ-Prefrontal (turquoise), and Rostral TPJ-Prefrontal (green) clusters, computed over trials of contacts, for Congruent trials (full lines) and Incongruent trials (dashed lines). A. In the Early Visual cluster, no significant Congruence effect was observed. B. In the Caudal TPJ – Prefrontal cluster activity in Congruent and Incongruent trials (IOR-related) differed significantly at 0.24-0.3s post target (shaded red areas; Congruence main effect: all $p_{correcte}horizontal_d<0.002$), and a significant hemispheric difference between IOR-related responses was observed at 0.14-.022s post target (shaded brown area; Hemisphere x Congruence interaction: all $p_{corrected}<0.03$). C. In the Rostral TPJ – Prefrontal cluster activity in Congruent and Incongruent trials differed significantly at 0.66-0.68s post target (green shaded area; Congruence main effect: all $p_{corrected}<0.003$). A-C. Shaded areas around traces depict SEM; Dashed vertical lines represent Target onset (black) and Cue onset (red) at the long-SOA condition; asterisks represent significant Congruence x Hemisphere post hoc comparisons ($p_{corrected}<0.05$). D. Typical examples of HFBB power IOR-related activity in the Congruent (full line) & Incongruent (dashed line) long-SOA conditions of single contacts of the Caudal TPJ-Prefrontal cluster.

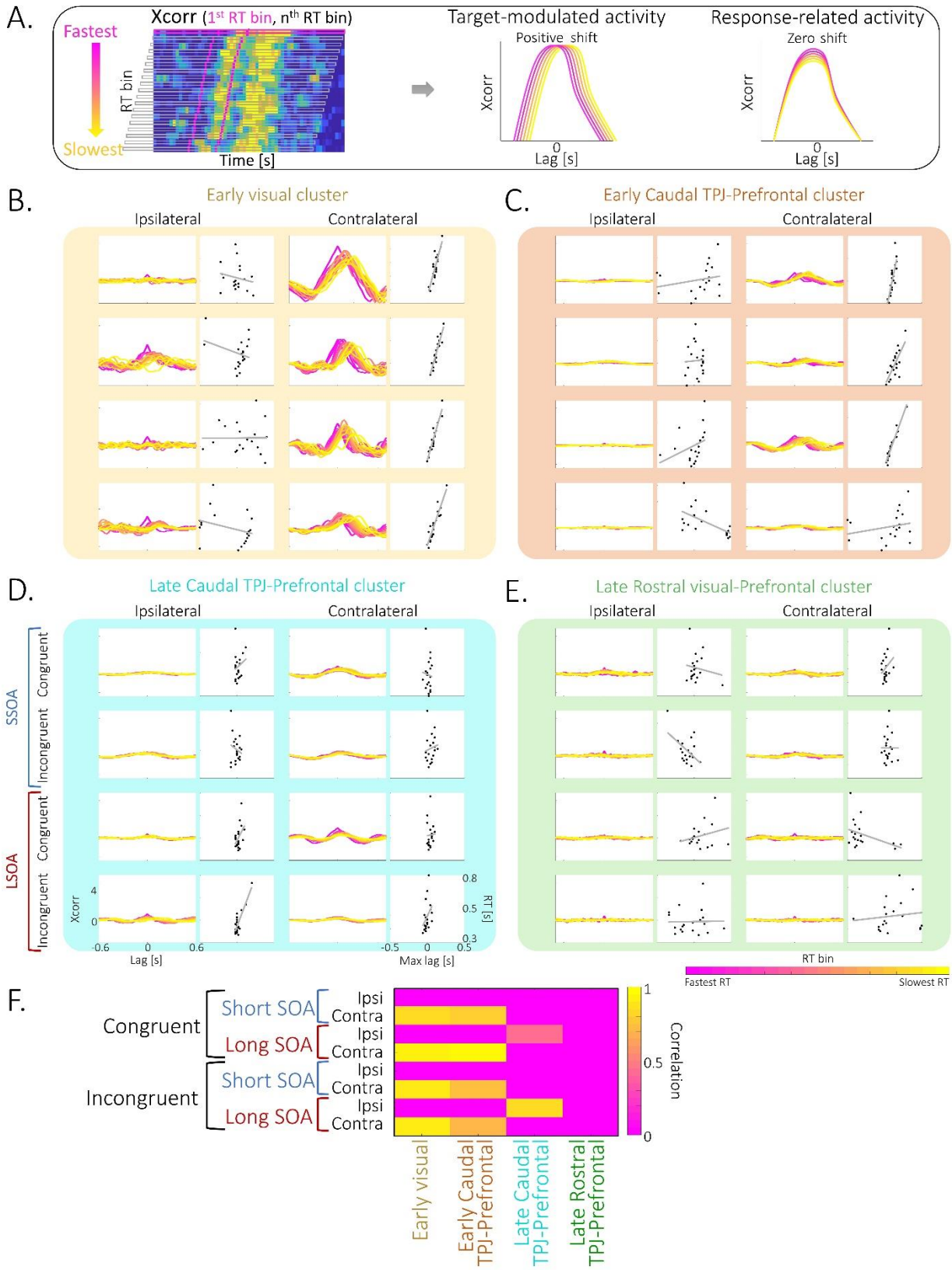
A.
Fastest
Slowest
Xcorr (1st RT bin, nth RT bin)
RT bin
Time [s]
Target-modulated activity
Positive shift
Xcorr
0
Lag [s]
Response-related activity
Zero shift
Xcorr
0
Lag [s]
B.
Early visual cluster
Ipsilateral
Contralateral
C.
Early Caudal TPJ-Prefrontal cluster
Ipsilateral
Contralateral
D.
Late Caudal TPJ-Prefrontal cluster
Ipsilateral
Contralateral
SSOA
Congruent
Incongruent
LSOA
Congruent
Incongruent
Xcorr
4
0
-0.6
0
0.6
Lag [s]
-0.5
0
0.5
Max lag [s]
0.8
0.5
0.3
RT [s]
E.
Late Rostral visual-Prefrontal cluster
Ipsilateral
Contralateral
RT bin
Fastest RT
Slowest RT
F.
Congruent
Short SOA
Ipsi
Contra
Long SOA
Ipsi
Contra
Incongruent
Short SOA
Ipsi
Contra
Long SOA
Ipsi
Contra
Early visual
Early Caudal TPJ-Prefrontal
Late Caudal TPJ-Prefrontal
Late Rostral TPJ-Prefrontal
1
0.5
0
Correlation

Figure S6 – Correlation of cluster response-locked neural activity with visual processing. A. Schematic illustration of the procedure for computing the cross-correlation (Xcorr) between response-locked neural activity across RT bins: Cross-correlation between response-locked activity at the fastest RT bin and all subsequent bins was computed (left). If cluster activity is target-associated, maximal cross-correlation will follow the RT (here indicative of quantile's mean target-onset time), resulting in a positive shift of cross-correlation lag (middle). If cluster activity is response-associated, maximal cross-correlation will be centered on target onset, resulting in a zero shift across all RT bins (right). B.-E. Cross-correlogram of response-locked neural activity at different RT bins (pink- fastest RT; yellow - slowest RT) as a function of cross-correlation lag (left columns), and Pearson correlation (grey line) between maximal cross-correlation lags (Max lag) and bin's mean target onsets (right columns), across the 8 conditions (Congruent / Incongruent X short-SOA / long-SOA X Ipsilateral target / contralateral target) for the Early visual (yellow), Early Caudal TPJ-Prefrontal (orange), Late Caudal TPJ-Prefrontal (turquoise) and Late Rostral TPJ-Prefrontal (green) clusters. B.-C. Early visual & Early Caudal TPJ-Prefrontal clusters' activity is target-associated: Cross-correlation plots are positively shifted in a spatially sensitive manner, i.e. only for contralateral targets. D.-E. Activity in the Late Caudal TPJ-Prefrontal & Late Rostral TPJ-Prefrontal clusters is response-associated: Cross-correlation plots show no shift. F. Significant positive correlation between cross-correlation maximal lag and bin mean RT in the Early visual & Early Caudal TPJ-Prefrontal clusters: significant ($p<0.05$) positive correlations were found mainly in these two clusters, only for contralateral targets.

References

1. J. Lupiáñez, in *Attention and Time*, A. C. Nobre, J. T. Coulle, Eds. (Oxford University Press, 2010), pp. 17–34.

2. M. I. Posner, Y. Cohen, in *Attention and performance X: Control of language processes*, H. Bouma, D. Bouwhuis, Eds. (Erlbaum, Hillsdale, NJ, 1984), pp. 531–56.

3. J. Lupiáñez, R. M. Klein, P. Bartolomeo, Inhibition of return: Twenty years after. *Cogn. Neuropsychol.* **23**, 1003–1014 (2006).

4. T. S. Malkinson, A. Bourgeois, N. Wattiez, P. Pouget, P. Bartolomeo, Evidence Accumulation Modelling Reveals that Gaussian Noise Accounts for Inhibition of Return. *Cold Spring Harbor Laboratory* (2020), p. 2020.06.21.163485, , doi:10.1101/2020.06.21.163485.

5. A. Sapir, N. Soroker, A. Berger, A. Henik, Inhibition of return in spatial attention: direct evidence for collicular generation. *Nat. Neurosci.* **2**, 1053–1054 (1999).

6. M. C. Dorris, R. M. Klein, S. Everling, D. P. Munoz, Contribution of the primate superior colliculus to inhibition of return. *J. Cogn. Neurosci.* **14**, 1256–1263 (2002).

7. K. Mirpour, F. Arcizet, W. S. Ong, J. W. Bisley, Been there, seen that: a neural mechanism for performing efficient visual search. *J. Neurophysiol.* **102**, 3481–3491 (2009).

8. K. Mirpour, Z. Bolandnazar, J. W. Bisley, Neurons in FEF Keep Track of Items That Have Been Previously Fixated in Free Viewing Visual Search. *J. Neurosci.* **39**, 2114–2124 (2019).

9. A. Bourgeois, A. B. Chica, A. Valero-Cabre, P. Bartolomeo, Cortical control of inhibition of return: Causal evidence for task-dependent modulations by dorsal and ventral parietal regions. *Cortex*. **49**, 2229–2238 (2013).

10. A. Bourgeois, A. B. Chica, A. Valero-Cabre, P. Bartolomeo, Cortical control of Inhibition of Return: Exploring the causal contributions of the left parietal cortex. *Cortex*. **49**, 2927–2934 (2013).

11. T. Ro, A. Farnè, E. Chang, Inhibition of return and the human frontal eye fields. *Exp. Brain Res.* **150**, 290–296 (2003).

12. A. Bourgeois, A. B. Chica, R. Migliaccio, M. Thiebaut de Schotten, P. Bartolomeo, Cortical control of inhibition of return: evidence from patients with inferior parietal damage and visual neglect. *Neuropsychologia*. **50**, 800–809 (2012).

13. P. Bartolomeo, S. Chokron, E. Siéroff, Facilitation instead of inhibition for repeated right-sided events in left neglect. *Neuroreport*. **10**, 3353–3357 (1999).

14. P. Bartolomeo, E. Siéroff, C. Decaix, S. Chokron, Modulating the attentional bias in unilateral neglect: The effects of the strategic set. *Exp. Brain Res.* **137**, 424–431 (2001).

15. R. Mukamel, I. Fried, Human intracranial recordings and cognitive neuroscience. *Annu. Rev. Psychol.* **63**, 511–537 (2012).

16. A. B. Chica, E. Martín-Arévalo, F. Botta, J. Lupiánez, The Spatial Orienting paradigm: How to design and interpret spatial attention experiments. *Neurosci. Biobehav. Rev.* **40**, 35–51 (2014).

17. D. S. Margulies, S. S. Ghosh, A. Goulas, M. Falkiewicz, J. M. Huntenburg, G. Langs, G. Bezgin, S. B. Eickhoff, F. X. Castellanos, M. Petrides, E. Jefferies, J. Smallwood, Situating the default-mode network along a principal gradient of macroscale cortical organization. *Proc. Natl. Acad. Sci. U. S. A.* **113**, 12574–12579 (2016).

18. M. Corbetta, G. L. Shulman, Control of goal-directed and stimulus-driven attention in the brain. *Nat. Rev. Neurosci.* **3**, 201–215 (2002).

19. R. F. Helfrich, I. C. Fiebelkorn, S. M. Szczepanski, J. J. Lin, J. Parvizi, R. T. Knight, S. Kastner, Neural Mechanisms of Sustained Attention Are Rhythmic. *Neuron*. **99**, 854-865.e5 (2018).

20. T. J. Buschman, S. Kastner, From Behavior to Neural Dynamics: An Integrated Theory of Attention. *Neuron*. **88**, 127–144 (2015).

21. M. Thiebaut de Schotten, F. Dell'Acqua, S. J. Forkel, A. Simmons, F. Vergani, D. G. M. Murphy, M. Catani, A lateralized brain network for visuospatial attention. *Nat. Neurosci.* **14**, 1245–1246 (2011).

22. R. B. Mars, J. Sallet, U. Schüffelgen, S. Jbabdi, I. Toni, M. F. Rushworth, Connectivity-based subdivisions of the human right "temporoparietal junction area": evidence for different areas participating in different cortical networks. *Cereb. Cortex*. **22**, 1894–1903 (2012).

23. P. Bartolomeo, T. Seidel Malkinson, Hemispheric lateralization of attention processes in the human brain. *Curr Opin Psychol*. **29**, 90–96 (2019).

24. T. Hattori, K. Ito, C. Nakazawa, Y. Numasawa, M. Watanabe, S. Aoki, H. Mizusawa, S. Ishiai, T. Yokota, Structural connectivity in spatial attention network: reconstruction from left hemispatial neglect. *Brain Imaging Behav.* **12**, 309–323 (2018).

25. M. Thiebaut de Schotten, M. Urbanski, H. Duffau, E. Volle, R. Levy, B. Dubois, P. Bartolomeo, Direct evidence for a parietal-frontal pathway subserving spatial awareness in humans. *Science*. **309**, 2226–2228 (2005).

26. J. M. Huntenburg, P.-L. Bazin, D. S. Margulies, Large-Scale Gradients in Human Cortical Organization. *Trends Cogn. Sci.* **22**, 21–31 (2018).

27. R. Gao, R. L. van den Brink, T. Pfeffer, B. Voytek, Neuronal timescales are functionally dynamic and shaped by cortical microarchitecture. *Elife*. **9** (2020), doi:10.7554/eLife.61277.

28. U. Hasson, E. Yang, I. Vallines, D. J. Heeger, N. Rubin, A hierarchy of temporal receptive windows in human cortex. *J. Neurosci.* **28**, 2539–2550 (2008).

29. S. J. Kiebel, J. Daunizeau, K. J. Friston, A hierarchy of time-scales and the brain. *PLoS Comput. Biol.* **4**, e1000209 (2008).

30. K. D. Himberger, H.-Y. Chien, C. J. Honey, Principles of Temporal Processing Across the Cortical Hierarchy. *Neuroscience*. **389**, 161–174 (2018).

31. A. Stigliani, B. Jeska, K. Grill-Spector, Encoding model of temporal processing in human visual cortex. *Proc. Natl. Acad. Sci. U. S. A.* **114**, E11047–E11056 (2017).

32. J. Zhou, N. C. Benson, K. N. Kay, J. Winawer, Compressive Temporal Summation in Human Visual Cortex. *J. Neurosci.* **38**, 691–709 (2018).

33. T. Seidel Malkinson, P. Bartolomeo, Fronto-parietal organization for response times in inhibition of return: The FORTIOR model. *Cortex*. **102**, 176–192 (2018).

34. H. M. Krüger, W. J. MacInnes, A. R. Hunt, Perceptual merging contributes to cueing effects. *J. Vis.* **14** (2014), doi:10.1167/14.7.13.

35. R. S. Desikan, F. Ségonne, B. Fischl, B. T. Quinn, B. C. Dickerson, D. Blacker, R. L. Buckner, A. M. Dale, R. P. Maguire, B. T. Hyman, M. S. Albert, R. J. Killiany, An automated labeling system for subdividing the human cerebral cortex on MRI scans into gyral based regions of interest. *Neuroimage*. **31**, 968–980 (2006).

A.

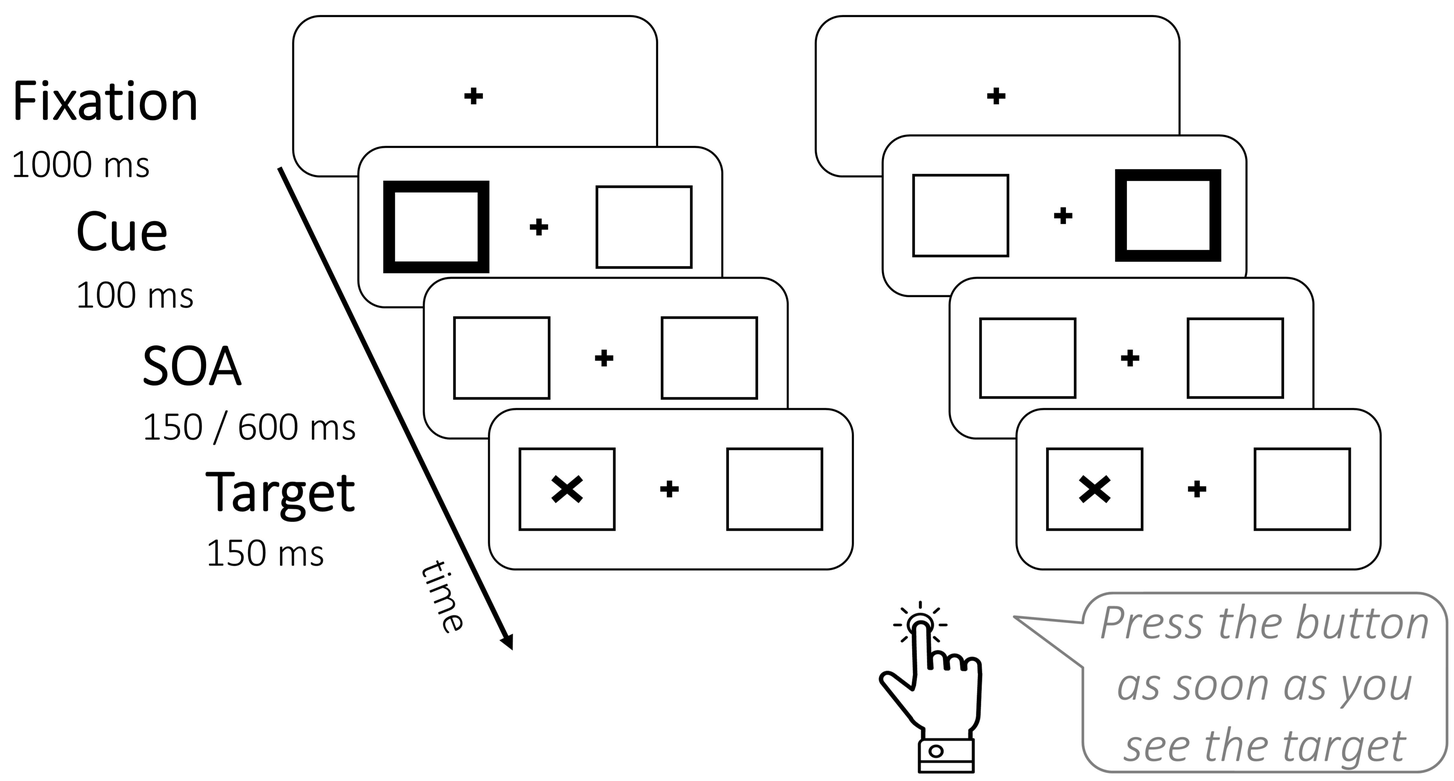
Congruent
Incongruent
Fixation
1000 ms
Cue
100 ms
SOA
150 / 600 ms
Target
150 ms
time
Press the button as soon as you see the target

B.

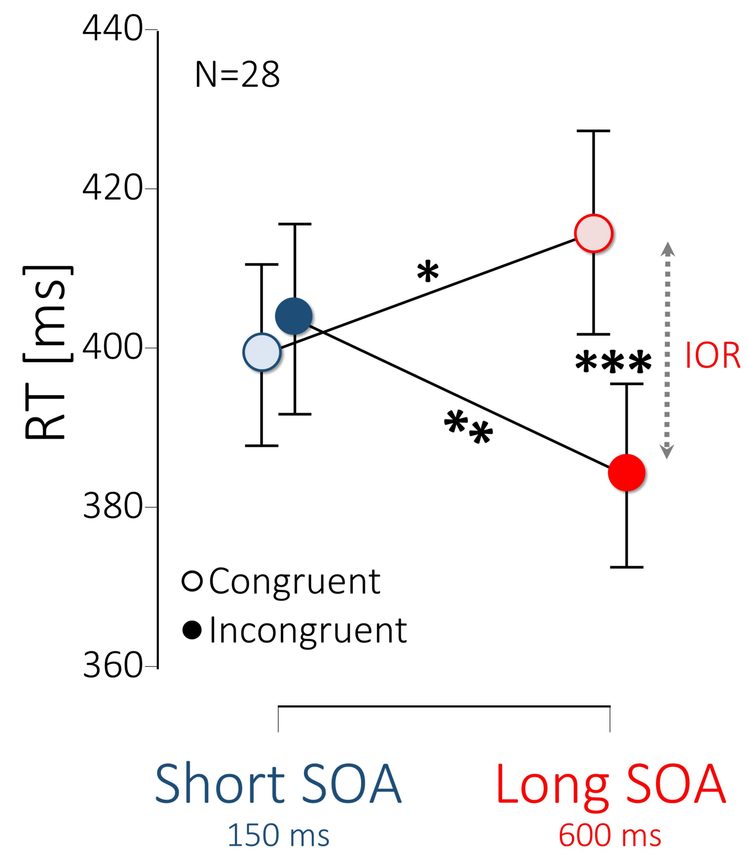
N=28
RT [ms]
440
420
400
380
360
*
***
**
IOR
Congruent
Incongruent
Short SOA
150 ms
Long SOA
600 ms

C.

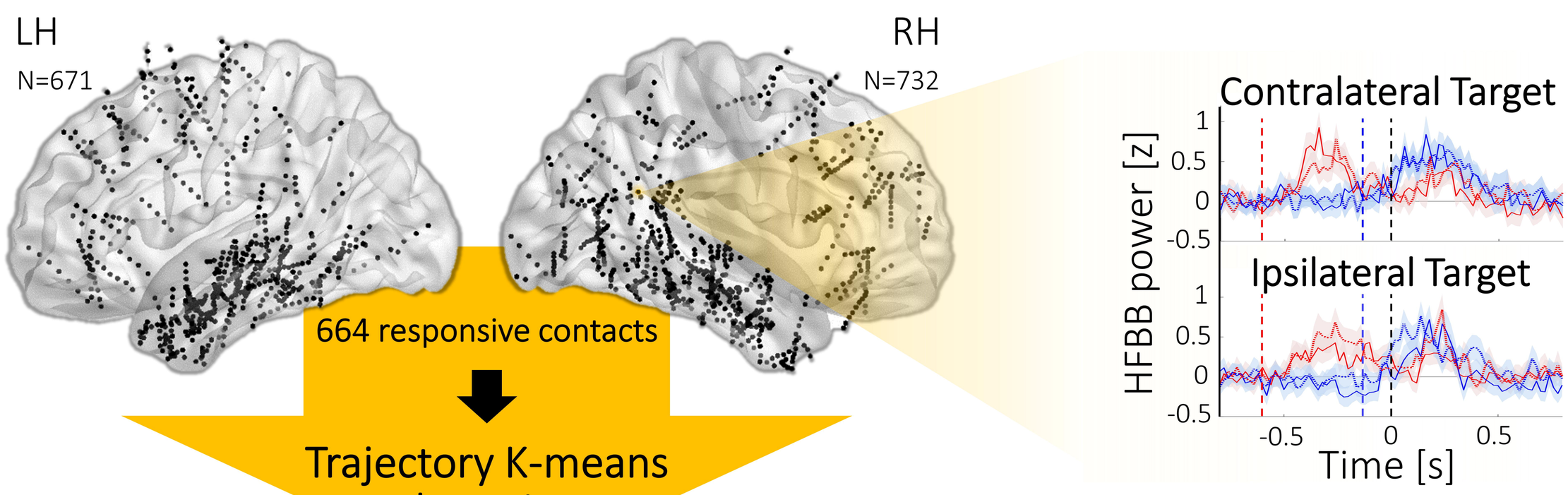
LH
N=671
RH
N=732
664 responsive contacts
Trajectory K-means clustering
Contralateral Target
Ipsilateral Target
HFBB power [z]
1
0.5
0
-0.5
-0.5
0
0.5
Time [s]

D.

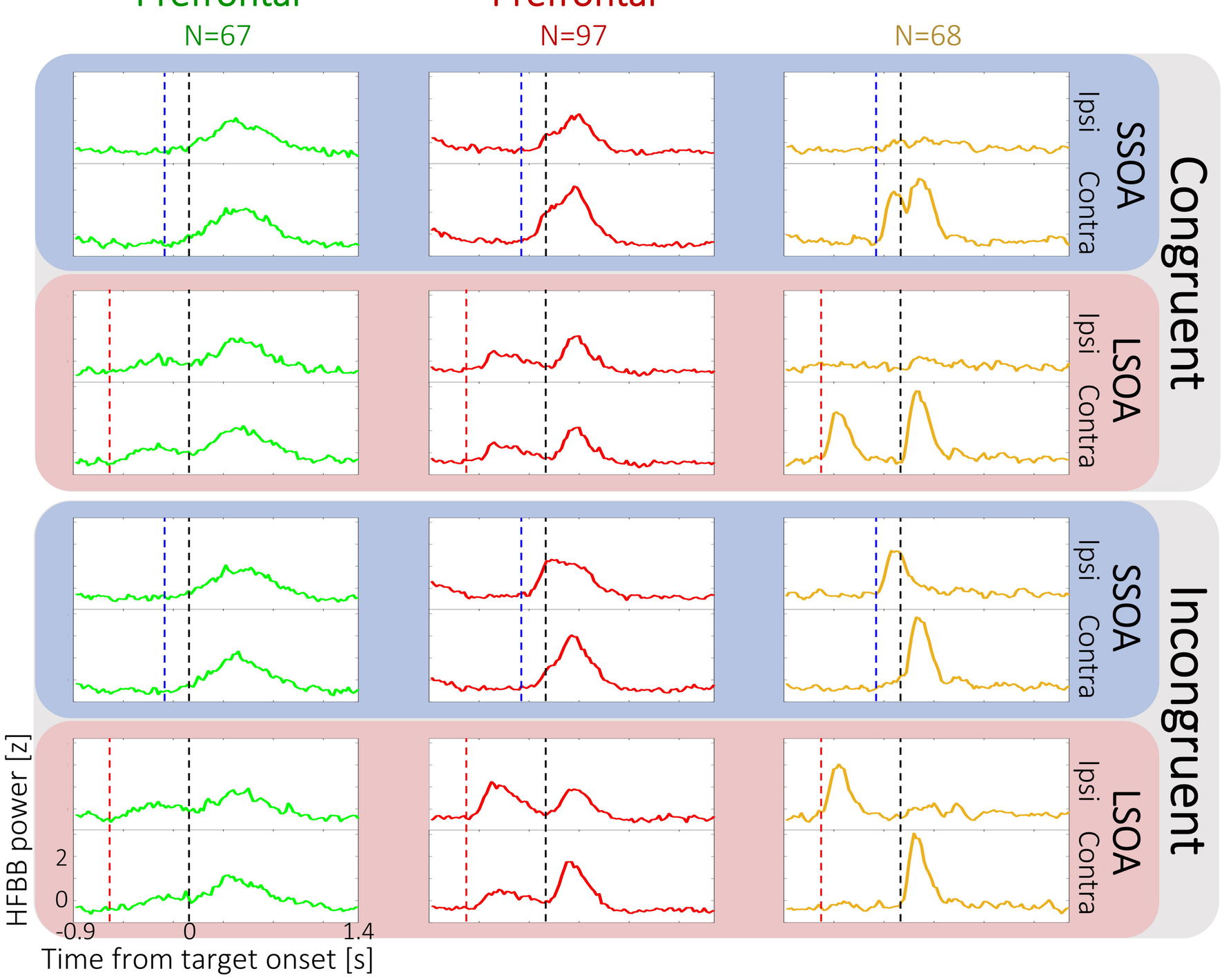
Rostral TPJ Prefrontal
N=67
Caudal TPJ Prefrontal
N=97
Visual
N=68
Congruent
Incongruent
SSOA
LSOA
Ipsi
Contra
HFBB power [z]
2
0
-0.9
0
1.4
Time from target onset [s]

E.

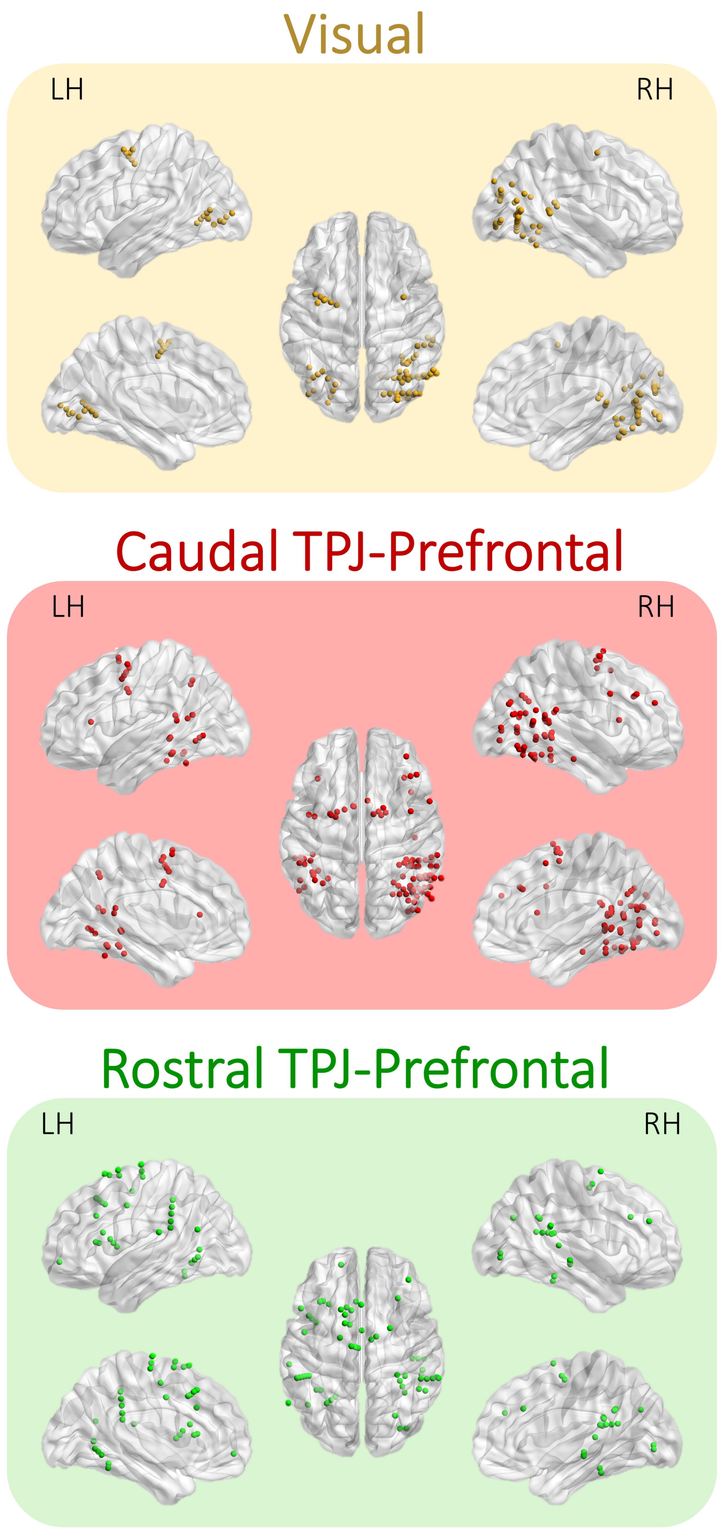
Visual
LH
RH
Caudal TPJ-Prefrontal
LH
RH
Rostral TPJ-Prefrontal
LH
RH

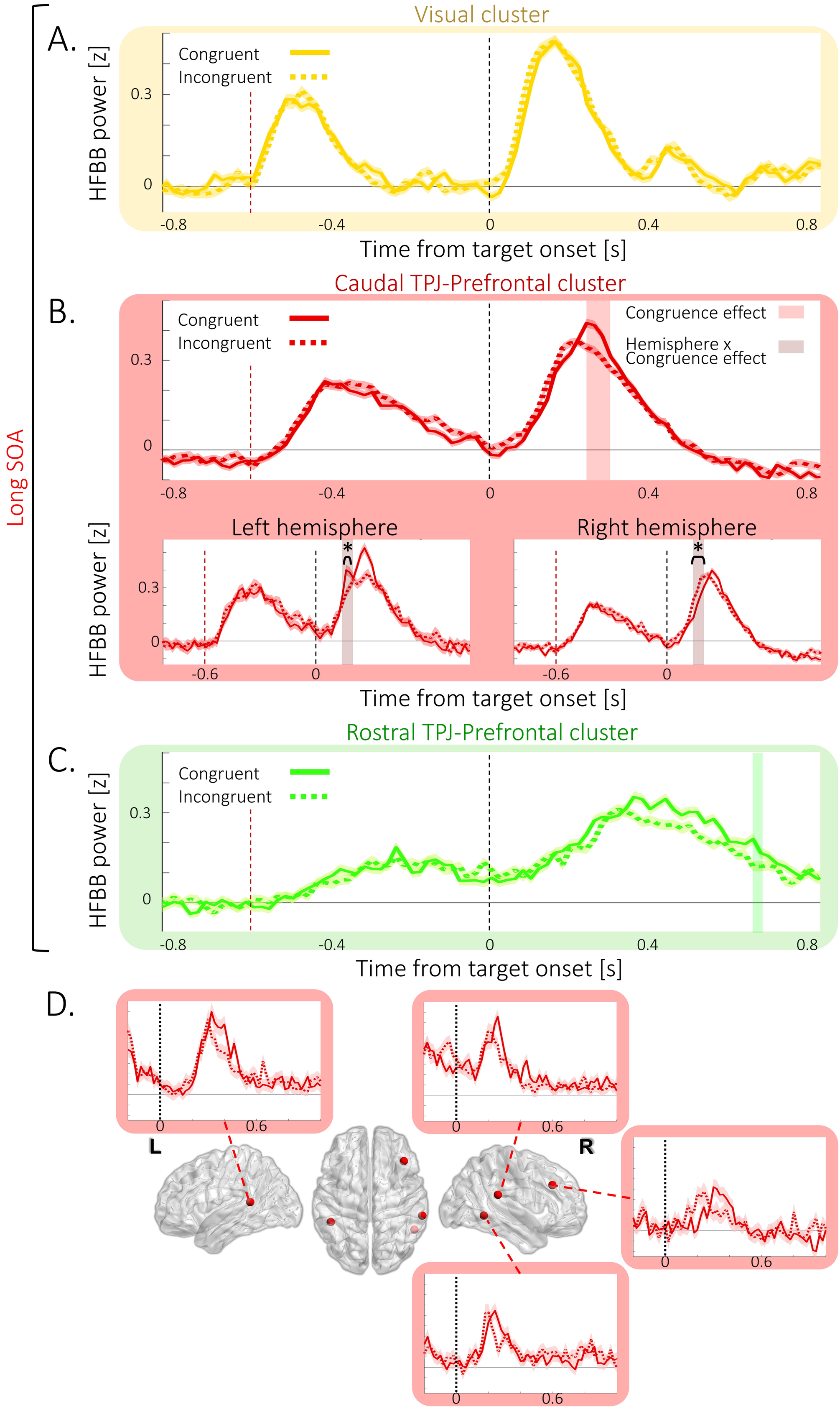
Long SOA
A.
Visual cluster
Congruent
Incongruent
HFBB power [z]
0.3
0
-0.8
-0.4
0
0.4
0.8
Time from target onset [s]
B.
Caudal TPJ-Prefrontal cluster
Congruent
Incongruent
Congruence effect
Hemisphere x Congruence effect
Left hemisphere
Right hemisphere
*
*
-0.6
0
C.
Rostral TPJ-Prefrontal cluster
D.
L
R

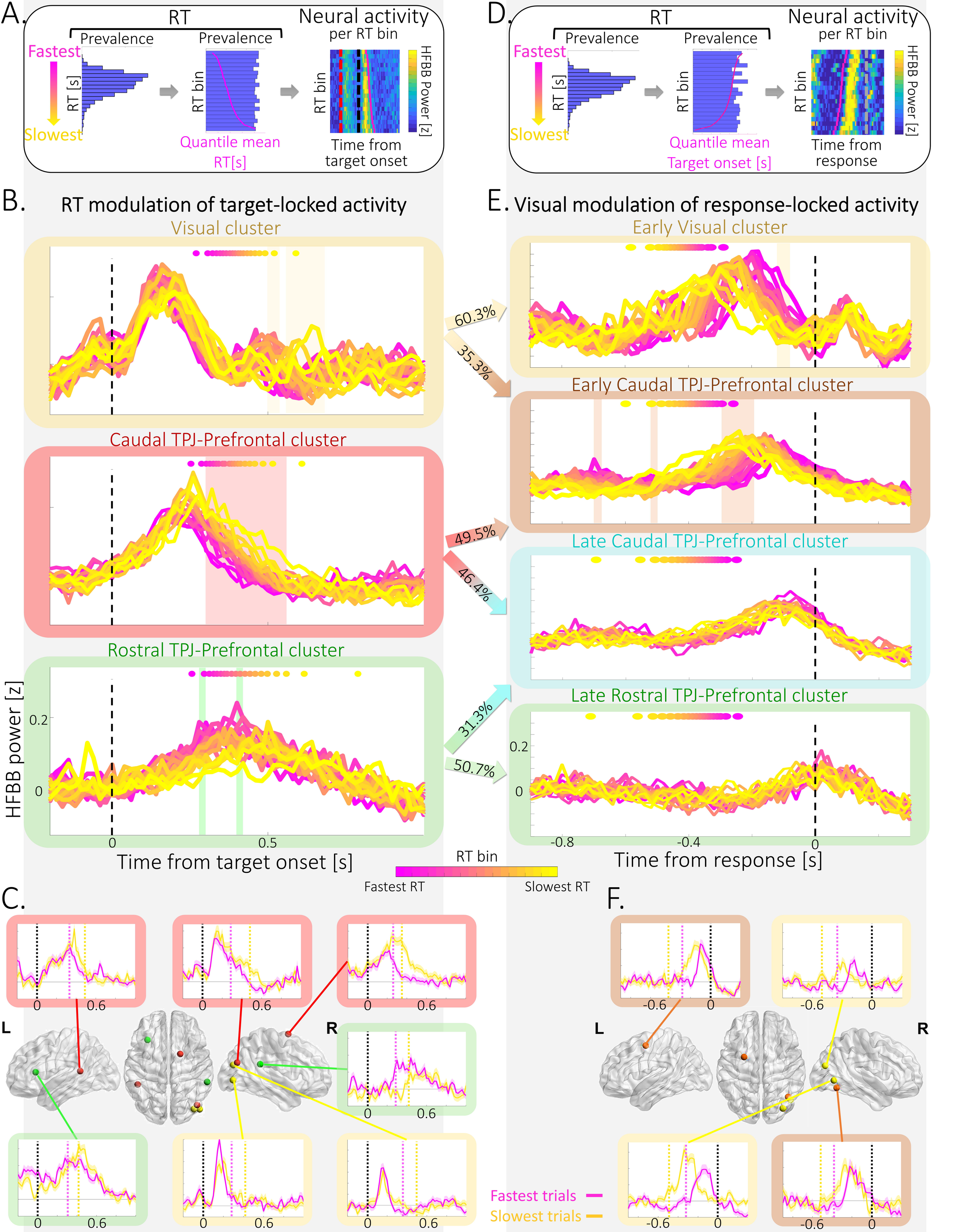
A.
RT
Prevalence
Prevalence
Neural activity
per RT bin
Fastest
Slowest
RT [s]
RT bin
Quantile mean
RT[s]
RT bin
Time from
target onset
HFBB Power [z]
D.
RT
Prevalence
Prevalence
Neural activity
per RT bin
Fastest
Slowest
RT [s]
RT bin
Quantile mean
Target onset [s]
RT bin
Time from
response
HFBB Power [z]
B.
RT modulation of target-locked activity
Visual cluster
Caudal TPJ-Prefrontal cluster
Rostral TPJ-Prefrontal cluster
HFBB power [z]
0.2
0
0
0.5
Time from target onset [s]
E.
Visual modulation of response-locked activity
Early Visual cluster
Early Caudal TPJ-Prefrontal cluster
Late Caudal TPJ-Prefrontal cluster
Late Rostral TPJ-Prefrontal cluster
60.3%
35.3%
49.5%
46.4%
31.3%
50.7%
0.2
0
-0.8
-0.4
0
Time from response [s]
RT bin
Fastest RT
Slowest RT
C.
L
R
0
0.6
F.
L
R
-0.6
0
Fastest trials
Slowest trials

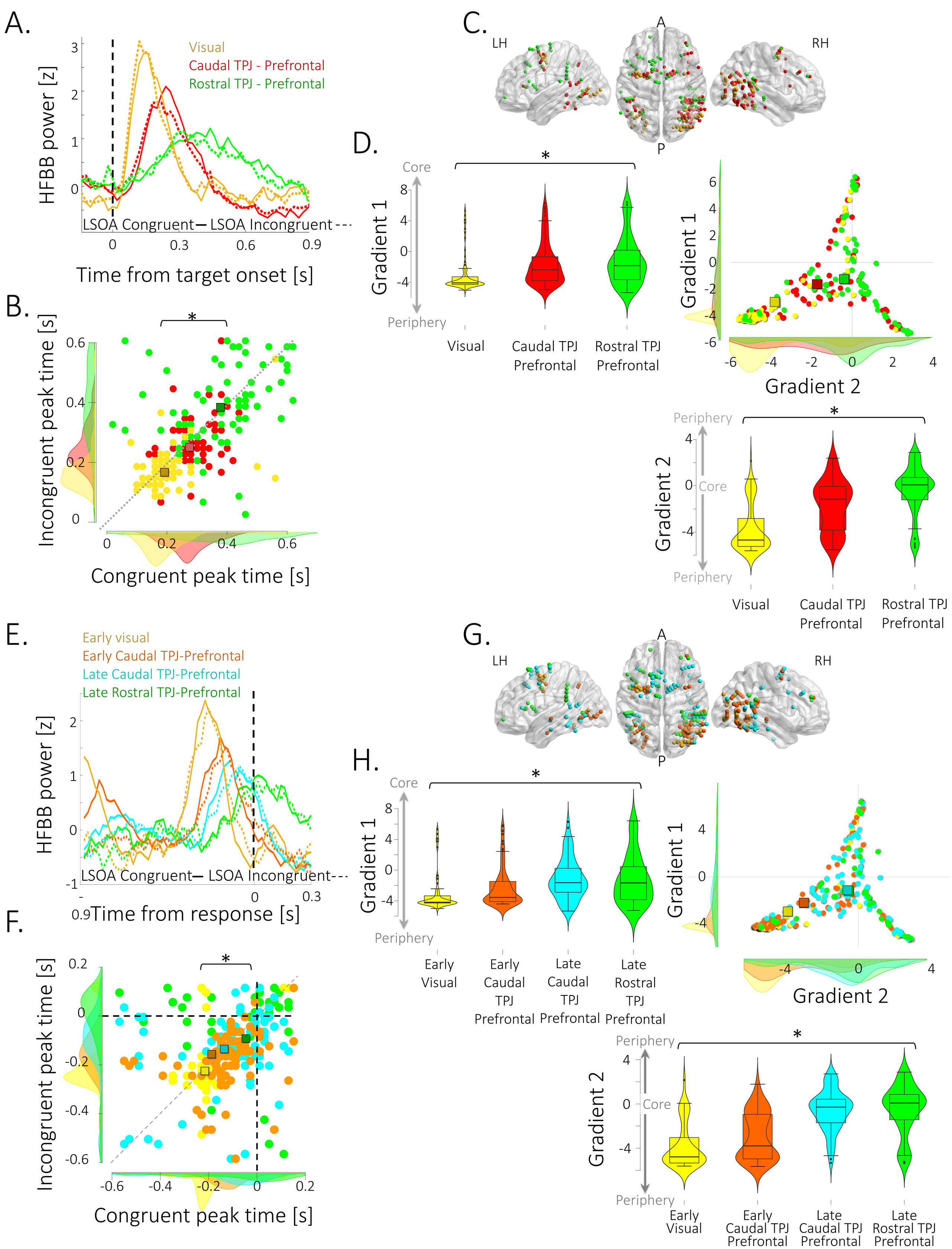
A.
Visual
Caudal TPJ - Prefrontal
Rostral TPJ - Prefrontal
HFBB power [z]
LSOA Congruent
LSOA Incongruent
Time from target onset [s]
B.
Incongruent peak time [s]
Congruent peak time [s]
C.
LH
RH
A
P
D.
Core
Periphery
Gradient 1
Visual
Caudal TPJ Prefrontal
Rostral TPJ Prefrontal
Gradient 2
E.
Early visual
Early Caudal TPJ-Prefrontal
Late Caudal TPJ-Prefrontal
Late Rostral TPJ-Prefrontal
HFBB power [z]
LSOA Congruent
LSOA Incongruent
Time from response [s]
F.
Incongruent peak time [s]
Congruent peak time [s]
G.
LH
RH
A
P
H.
Core
Periphery
Gradient 1
Early Visual
Early Caudal TPJ Prefrontal
Late Caudal TPJ Prefrontal
Late Rostral TPJ Prefrontal
Gradient 2